Avalanches and the directed percolation depinning model: Experiments, simulations, and theory

L. A. N. Amaral,[1] A.-L. Barabási,[1,*] S. V. Buldyrev,[1] S. T. Harrington,[1] S. Havlin,[1,2]
R. Sadr-Lahijany,[1] and H. E. Stanley[1]
[1] *Center for Polymer Studies and Department of Physics, Boston University, Boston, Massachusetts 02215*
[2] *Minerva Center and Department of Physics, Bar-Ilan University, Ramat Gan, Israel*
(Received 8 December 1994)

We study the recently introduced directed percolation depinning (DPD) model for interface roughening with quenched disorder for which the interface becomes pinned by a directed percolation (DP) cluster for $d = 1$ or a directed surface for $d > 1$. The mapping to DP enables us to predict some of the critical exponents of the growth process. For the case of $1+1$ dimensions, the theory predicts that the roughness exponent α is given by $\alpha = \nu_\perp/\nu_\parallel$, where $\nu_\perp$ and $\nu_\parallel$ are the exponents governing the divergence of perpendicular and parallel correlation lengths of the DP incipient infinite cluster. The theory also predicts that the dynamical exponent z equals the exponent $d_{\min}$ characterizing the scaling of the shortest path on an isotropic percolation cluster. For the case of $1+1$ dimensions, our simulations give $\nu_\parallel = 1.73 \pm 0.02$, $\alpha = 0.63 \pm 0.01$, and $z = 1.01 \pm 0.02$, in good agreement with the theory. For the case of $2+1$ dimensions, we find $\nu_\parallel = 1.16 \pm 0.05$, $\alpha = 0.48 \pm 0.03$, and $z = 1.15 \pm 0.05$, also in accord with the theory. For higher dimensions, α decreases monotonically but does not seem to approach zero for any dimension calculated ($d \leq 6$), suggesting that the DPD model has no upper critical dimension for the static exponents. On the other hand, z appears to approach 2 as $d \to 6$, as expected by the result $z = d_{\min}$, suggesting that $d_c = 6$ for the dynamics. We also perform a set of imbibition experiments, in both $1+1$ and $2+1$ dimensions, that can be used to test the DPD model. We find good agreement between experimental, theoretical, and numerical approaches. Further, we study the properties of avalanches in the context of the DPD model. In $1+1$ dimensions, our simulations for the critical exponent characterizing the duration of the avalanches give $\tau_{\text{surv}} = 1.46 \pm 0.02$ and for the exponent characterizing the number of growth cells in the interface $\delta = 0.60 \pm 0.03$. In $2+1$ dimensions, we find $\tau_{\text{surv}} = 2.18 \pm 0.03$ and $\delta = 1.14 \pm 0.06$. We relate the scaling properties of the avalanches in the DPD model to the scaling properties for the self-organized depinning model, a variant of the DPD model. We calculate the exponent characterizing the avalanches distribution τ_{aval} for $d = 1$–6 and compare our results with recent theoretical predictions. Finally, we discuss a variant of the DPD model, the "gradient DPD model," in which the concentration of pinning cells increases with height. We perform a set of experiments in $1+1$ dimensions that are well described by the gradient DPD model.

PACS number(s): 47.55.Mh, 68.35.Fx

I. INTRODUCTION

Recently the growth of rough interfaces has witnessed an explosion of theoretical, numerical, and experimental studies, fueled by the broad interdisciplinary aspects of the subject [1–6]. Applications can be so diverse as imbibition in porous media, fluid-fluid displacement, bacterial colony growth, fire front motion, and the motion of flux lines in superconductors [7–17].

In general, a d-dimensional self-affine interface, described by a single-valued function $h(x,t)$, evolves in a $(d+1)$-dimensional medium. Usually, some form of disorder η affects the motion of the interface leading to its roughening. Two main classes of disorder have been discussed in the literature. The first, called thermal or "annealed," depends only on time. The second, referred to as "quenched," is frozen in the medium. Early studies focused on time-dependent uncorrelated disorder as being responsible for the roughening. Here we focus on the effect of quenched disorder on the growth.

The roughening process can be quantified by studying the *global* interface width

$$W(L,t) \equiv \left\langle \left[\overline{h^2(\mathbf{x},t)} - \overline{h(\mathbf{x},t)}^2 \right]^{1/2} \right\rangle, \qquad (1.1)$$

where L is the system size, the overbar denotes a spatial average, and the angular brackets denote an average over realizations of the disorder. The study of discrete models [18–21] and continuum growth equations [22,23] leads to the observation that during the initial period of the growth, i.e., for $t \ll t_\times(L)$, the width grows with time as

$$W(t) \sim t^\beta \qquad (t \ll t_\times), \qquad (1.2)$$

where β is the *growth* exponent. For times much larger than $t_\times$, the width saturates to a constant value. It was observed that the saturation width of the interface W_{sat} scales with L as

*Present address: T. J. Watson Research Center, P.O. Box 218, Yorktown Heights, NY 10598.

$$W_{\rm sat} \sim L^{\alpha} \qquad (t \gg t_{\times}), \tag{1.3}$$

where α is the *roughness* exponent. The dependence of $t_{\times}$ on L allows the combination of (1.2) and (1.3) into a single scaling law [18]

$$W(L,t) \sim L^{\alpha}\, f_1(t/t_{\times}), \tag{1.4a}$$

where

$$t_{\times} \sim L^{z}. \tag{1.4b}$$

Here $z = \alpha/\beta$ is the *dynamical* exponent and $f_1(u)$ is a universal scaling function that grows as u^{β} when $u \ll 1$ and approaches a constant when $u \gg 1$.

An alternative way of determining the scaling exponents is to study the *local* width w in a window of observation of length $\ell < L$. The scaling law (1.4b) and the fact that the interface is self-affine allow us to conclude

$$w(\ell,t) \sim \ell^{\alpha}\, f_2(\ell/\ell_{\times}), \tag{1.5a}$$

where

$$\ell_{\times} \sim t^{1/z} \qquad (t \ll t_{\times}), \tag{1.5b}$$

or

$$\ell_{\times} \sim L \qquad (t \gg t_{\times}). \tag{1.5c}$$

Here $f_2(u)$ is a universal scaling function that decreases as $u^{-\alpha}$ when $u \gg 1$ and approaches a constant when $u \ll 1$.

The simulation of discrete models [18–21] gives exponents in agreement with the predictions of phenomenological continuum approaches, such as the Edwards-Wilkinson (EW) equation [22] and the Kardar-Parisi-Zhang (KPZ) equation [23]. However, experimental studies find exponents significantly larger than the predictions of theory, for example, for $1+1$ dimensions, Refs. [22,23] predict $\alpha = 1/2$, but experiments show $\alpha \simeq 0.6 - 1.0$ [7–17]. Although various explanations were proposed — long-range correlations [24], power-law distribution [25] for the disorder, or coupling of the interface to impurities [26] — it is currently accepted that *quenched* disorder plays an essential role in those experiments [13–17,27–41].

The presence of quenched disorder allows an interesting analogy with critical phenomena. The continual motion of the interface requires the application of a driving force F. There exists a critical value F_c such that for $f < F_c$, the interface will become pinned by the disorder after some finite time. For $F > F_c$ the interface moves indefinitely with a constant velocity v. This means that the motion of driven rough interfaces in disordered media can be studied as a phase transition — called the depinning transition. The velocity of the interface v plays the role of the *order parameter*, since as $F \to F_c^+$, v vanishes as

$$v \sim f^{\theta}, \tag{1.6}$$

where θ is the *velocity* exponent and $f \equiv (F - F_c)/F_c$ is the *reduced force* (Fig. 1).

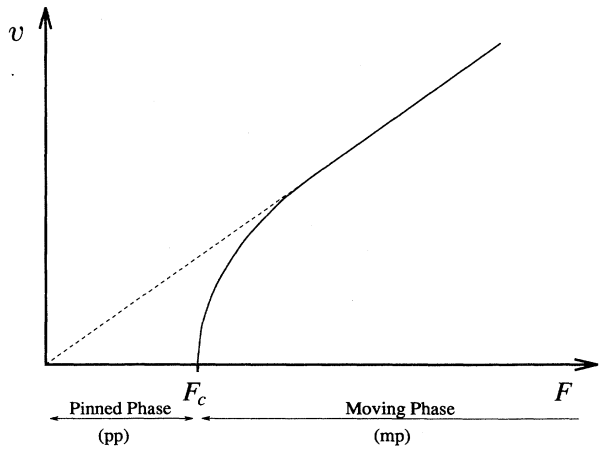

FIG. 1. Depinning transition. In the "pinned phase" (PP) $F < F_c$, the velocity of the interface is zero. In the "moving phase" (MP) $F > F_c$, the interface moves with a constant average velocity v. The velocity plays the role of the order parameter of the transition.

For $F \to F_c^+$, large but finite regions of the interface are pinned by the disorder. At the transition, the characteristic length ξ of these pinned regions diverges,

$$\xi \sim f^{-\nu}, \tag{1.7}$$

where ν is the *correlation length* exponent.

Several models in which quenched disorder plays an essential role have been proposed recently [13–17,27–41]. For one class of models [13,14,27], in $1+1$ dimensions, α can be obtained exactly by mapping the interface, at the depinning transition onto *directed percolation* (DP). In higher dimensions the interface can be mapped to a *directed surface* (DS) [15]. In $1+1$ dimensions, DP and DSs are equivalent. We refer to this class of models as the *directed percolation depinning* (DPD) universality class.

Recent numerical studies [37], confirmed by analytical arguments [38], showed that this class of models can be described by a stochastic differential equation of the KPZ type [36]

$$\frac{\partial h}{\partial t} = F + \nabla^2 h + \lambda(\nabla h)^2 + \eta(\mathbf{x},h), \tag{1.8}$$

where $\eta(\mathbf{x},h)$ represents the quenched disorder and the coefficient λ of the nonlinear term diverges at the depinning transition [37]. This equation was originally proposed in the context of interface roughening in the presence of quenched disorder in Ref. [36]. The numerical integration of (1.8) yielded exponents in agreement with the calculations for the models in the DPD universality class [36].

For a number of different models [28–33,39] belonging to a second universality class — referred to as *isotropic growth* — we have either $\lambda = 0$ or $\lambda \to 0$ at the depinning transition [37]. So, near the depinning transition, they can be described by an equation of the EW type with quenched disorder [42]

$$\frac{\partial h}{\partial t} = F + \nabla^2 h + \eta(\mathbf{x}, h). \quad (1.9)$$

This equation has been studied by means of the functional renormalization group [40,41], yielding $\alpha = \epsilon/3$, $\nu = 1/(2-\alpha)$, and $z = 2 - 2\epsilon/9$, where $\epsilon = 4 - d$.

When $F \gg F_c$, the size of the pinned regions in the interface ξ decreases to values much smaller than the system size L. For length scales ℓ larger than ξ, the quenched disorder becomes irrelevant and time-dependent noise dominates the roughening process. This means that for $\ell \gg \xi$ we should recover the results of either the EW or the KPZ equation with annealed noise (depending on the absence or the presence of nonlinear terms). This behavior has been observed both in experiments [7–12] and in simulations of discrete models [13–15,27–33,39].

The DPD model, discussed in this paper, was introduced in Refs. [13,14] to explain a set of simple imbibition experiments — a somewhat different model, belonging to the same universality class, was independently introduced in Ref. [27]. In these experiments, a colored suspension (coffee or ink) imbibes a sheet of paper, in the $(1+1)$-dimensional case, or a porous, spongelike brick, in the $(2+1)$-dimensional case [13–17]. The experimentally measured roughness exponents are in good agreement with the predictions of the DPD models [13–15,27]. However, a number of experimental features cannot be explained by this model. For example, in the experiments, the saturation width and the average height of the pinned interface depend on the rate of evaporation, which is not taken into account in the DPD model. We will also discuss a variant of the DPD model that enables us to explain the experimental results in terms of the effect of evaporation [17].

A self-organized variant of the DPD model has also been studied [13,43]. In this model the growth proceeds by avalanches, whose properties are not only of interest for the study of interface roughening [44–47], but also for other fields, including biological evolution in ecological systems [48–51].

The paper is organized as follows. In Sec. II we describe a set of imbibition experiments, in both $1+1$ dimensions and $2+1$ dimensions, that allow us to study the scaling properties of interface roughening in media with quenched disorder. In Sec. III we discuss the DPD model and calculate its relevant exponents. We analyze its mapping to DP for one-dimensional interfaces (and DSs, for higher dimensions) and its connection to the universality class of the KPZ equation with quenched disorder. In Sec. IV we define avalanches and discuss their scaling properties and their relation to the self-organized depinning (SOD) model. In Sec. V we describe a set of experiments that probe the "reason" for the pinning of the interface. We link this pinning to a gradient in the driving force generated by evaporation and the fluid properties. We find that the scaling of the interface width changes with the evaporation rate and is characterized by an exponent γ. We then introduce a variant of the DPD model that explains the experimental features and present the results of calculations for this model. Finally, in Sec. VI we summarize the main results of the paper. Some of the results were presented in a preliminary form in several conference proceedings [13,15,16].

II. IMBIBITION EXPERIMENTS

In this section we describe a set of experiments — originally proposed in Refs. [13–15] — that allow us to study the scaling properties of a rough interface moving in a disordered medium. In these experiments, a colored suspension imbibes an absorbing material, in $1+1$ dimensions a sheet of paper, and in $2+1$ dimensions a spongy brick or a paper roll.

A. The case of 1 + 1 dimensions

In the $(1+1)$-dimensional experiments, a sheet of paper with an edge of 20 cm is dipped into a reservoir filled with a colored suspension: coffee (see Fig. 2). A wet region starts to grow and a rough interface between dry and wet regions, the wetting front, propagates in the paper.

Although the experiments are quite simple to describe, the prediction of the scaling properties of the wetting

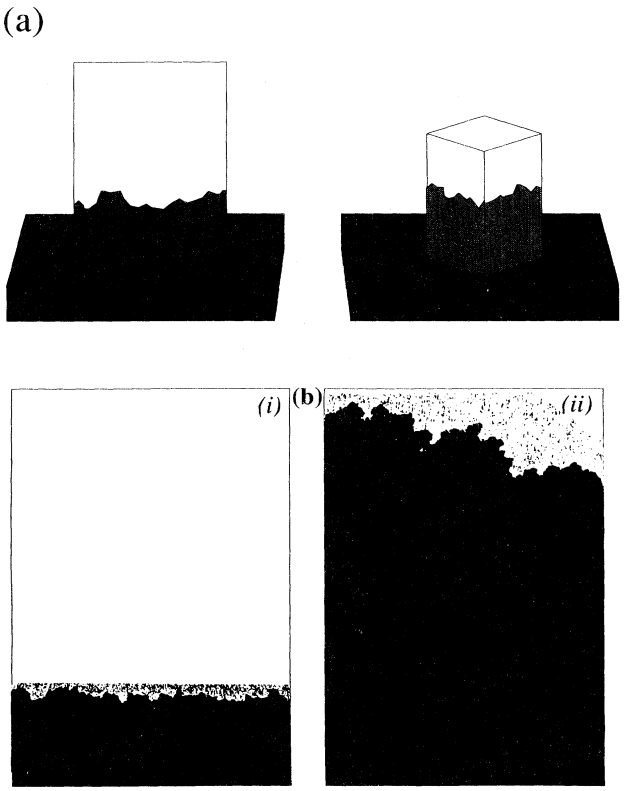

FIG. 2. (a) Schematic illustration of the experimental setup. In the $1+1$-dimensional experiments we use paper towels as the disordered media and coffee as the invading fluid. The edge of the paper towels is 20 cm. (b) Photographs of pinned interfaces in imbibition experiments with coffee and paper towels for (i) a high evaporation rate $g_{\rm expt} = 0.94 g_0$ and (ii) a low evaporation rate $g_{\rm expt} = 0.25 g_0$. Here g_0 is the undetermined multiplicative constant discussed in Sec. V.

front from first principles is very complex. At microscopic length scales, paper is an extremely disordered substance, formed by long fibers that are randomly distributed and connected. The wetting fluid propagates along the fibers of the paper due to capillary forces.

The advance of the wetting front depends on many factors: fluid density (which depends on the evaporation rate), suspension viscosity and density, gravity, temperature, size of the holes between fibers, etc. Some of these factors (evaporation rate, gravity, fluid density) modify the *effective* value of the driving force that leads to the advance of the wetting front. Other factors, such as the size of the holes between fibers, determine the pinning force that opposes the growth of the wet region.

Certain regions of the paper can locally pin the advance of the wet region. If such a region spans the entire system the interface can become globally pinned, so the advance of the wetting front is stopped [52]. As the interface departs from the water source, evaporation is constantly decreasing the fluid density, making it more and more difficult for the wetting front to advance. Eventually, a critical height h_c is reached for which the fluid pressure becomes such that the wetting of the regions above becomes impossible.

When the interface becomes pinned, we digitize the rough boundary between wet (colored) and dry (uncolored) areas. In Fig. 3 we plot the local width w (averaged over ten experiments) as a function of the window of observation ℓ for the digitized experimental interface. We observe a power-law scaling for nearly 1.5 decades. The fit to a power law, supported by consecutive slope analysis, results for the "pinned phase" in

$$\alpha^{p}_{\text{expt}} = 0.63 \pm 0.04 \qquad (d = 1). \tag{2.1}$$

We repeated the experiments, but this time not allowing enough time for the interface to get pinned. We then digitized the interface and plotted w against ℓ (Fig. 3). The best fit to a power law results for the "moving phase" in

$$\alpha^{m}_{\text{expt}} = 0.73 \pm 0.05 \qquad (d = 1). \tag{2.2}$$

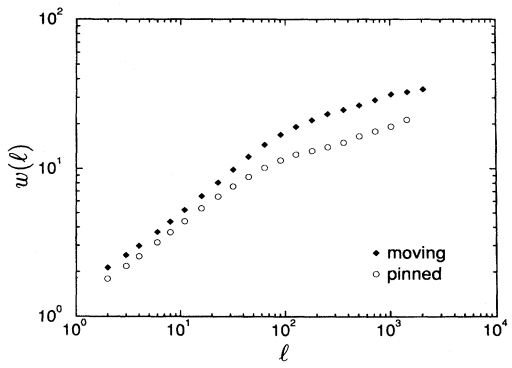

FIG. 3. Experimental local width w for the pinned and the moving interfaces in $1+1$ dimensions. It is visually apparent that the moving interface has a larger width and a different roughness exponent than the pinned interface.

Although the error bars show that the two values could be identical, the analysis of the DPD model in the next section suggests that they should be different.

B. The case of 2 + 1 dimensions

We perform two sets of experiments in 2+1 dimensions. In the first, we used an Oasis brick as the disordered medium. This brick is made of a spongelike material and is used by florists to absorb excess water. In the second set of experiments, we used a paper-towel roll. As the invading fluid, we tested several suspensions and found the most appropriate to be Bingo ink because of its high viscosity and good coloring.

To ensure good absorption of fluid by the spongy brick or the paper roll, we placed them over small ball bearings. In both sets of experiments, we added ink gradually and periodically, in order to maintain a fairly constant level of ink in the container.

Unfortunately, we could not be sure if the interface had in fact become pinned everywhere or not, but we always allowed enough time for the interface to propagate for several centimeters into the absorbing media. After the propagation period, we sliced the Oasis brick into longitudinal sections and digitized the rough interface. For the paper roll, we selected and digitized several sheets from different radii (Fig. 4).

We calculated the local width w for 13 slices of the brick and 9 sheets of paper. In Fig. 5 we show the average values of the local width for the brick and the paper roll. We find power-law scaling over roughly one decade. The best fit results in an exponent

$$\alpha_{\text{expt}} = 0.52 \pm 0.04 \qquad (d = 2). \tag{2.3}$$

When we compare this result with the calculations for the DPD model in $2+1$ dimensions, we will see that within the error bars is consistent with both the results for the pinned phase or the moving phase. In the $(1+1)$-

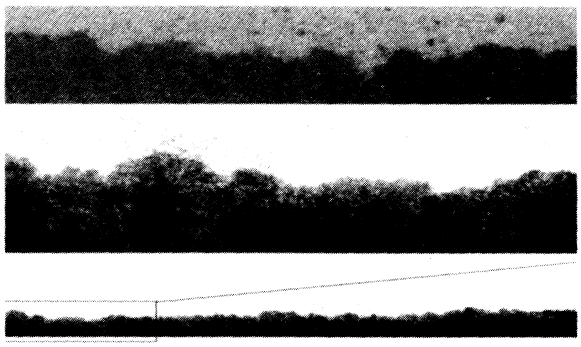

FIG. 4. Digitized ink interface in the (a) Oasis brick and (b) paper roll using an Apple computer scanner with a resolution of 300 pixels per inch. In (c) we show the full image from which (b) was magnified. The brick has a section of 7×7 cm^2 and the paper roll an exterior radius of 7.5 cm and an interior radius of 1.75 cm.

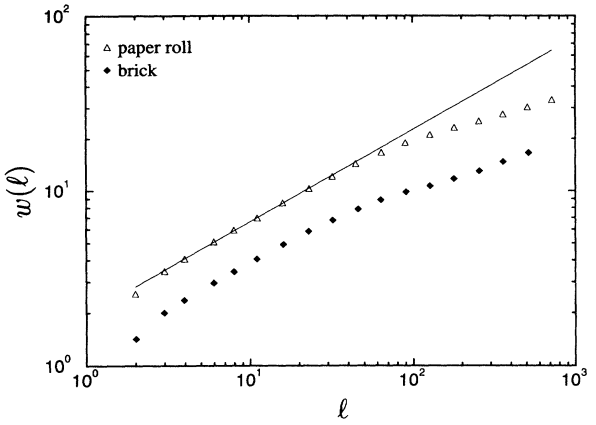

FIG. 5. Scaling of the local width w with ℓ for the experiments in $2+1$ dimensions. The curve for the paper roll results from averaging over 13 different paper sheets and the one for the Oasis brick results from averaging over 9 different sections.

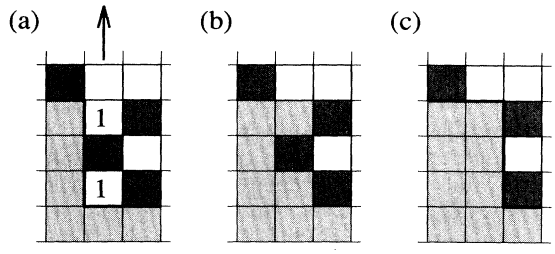

FIG. 6. Example of the application of the growth rule to a particular configuration of the interface. White squares refer to dry unblocked cells, the darker squares refer to dry blocked cells, and the gray squares refer to wet cells. The tick line shows the position of the interface. Let us suppose that the column indicated by the arrow in (a) was chosen for growth. According to our model, the cells marked 1 will become wet because they are nearest neighbors to the wet region. After the wetting, we can see in (b) that the cell marked 2 is below a wet cell, applying the rule to erode any overhang we wet that cell. In (c) we show the configuration of the interface after the growth (thick line).

dimensional experiments we are able to be certain that the interface is completely pinned when we digitize it. On the other hand, in the case of $2+1$ dimensions the interface may still be moving when we interrupt the experiments. In fact, in the case of $2+1$ dimensions, it is not clear if evaporation can have any role in the pinning of the interface.

III. THE DPD MODEL

The imbibition experiments described in the preceding section are too complex to be described from first-principles. For this reason it is convenient to develop a model that captures the most important features of the experiments. With this approach we lose the possibility of exactly predicting the form of the rough interface between the wet and the dry regions. Instead, we will be able to explain the scaling properties of the interface. The DPD model was initially introduced in Refs. [13,14] (and independently in Ref. [27]) with such intentions. The model was studied in more detail in Refs. [14–17,27].

In this section we will describe the DPD model in $1+1$ dimensions; the generalization for higher dimensions is immediate. We then proceed to discuss its most important properties. In Sec. IV we discuss the concept of avalanches in the DPD model and study their scaling properties.

A. Description of the model

Let us consider a square lattice of edge L with periodic boundary conditions along the direction of that edge. To each cell i of the lattice we assign an uncorrelated random number, the disorder η_i, with magnitude uniformly distributed in the interval $[0,1]$. The role of η_i is to model the random pinning forces generated by the disorder. We compare the random pinning forces η_i in the lattice with the driving force F, where $0 \leq F \leq 1$. If the pinning force at a certain cell η_i is larger than the driving force, the cell is labeled "blocked"; otherwise it is labeled "unblocked." Thus a cell is blocked with a probability

$$p = 1 - F. \tag{3.1}$$

Since the model was developed to study imbibition, we will refer to the growing, invading, region as "wet" and to the invaded region as "dry." At time $t = 0$, we wet all cells in the bottom row of the lattice. Then we select a column at random [53] and wet all dry *unblocked cells* in that column that are nearest neighbors to a wet cell. To obtain a single-valued interface, we impose the auxiliary rule that all dry *blocked cells* below a wet cell become wet as well [54] (see Fig. 6). We refer to this rule as *erosion of overhangs*. The time unit is defined as L growth attempts.

We define pinning clusters to be any group of blocked cells that are connected through nearest- or next-nearest-neighbor blocked cells. Any pinning cluster whose linear size ξ is smaller than the system size cannot prevent the advance of the interface. In fact, any pinning cluster that does not span the system will eventually become surrounded by the invading fluid, since the invading front can move around finite "obstacles," and the erosion of overhangs rule implies that after being surrounded the pinning cluster becomes wet.

B. Connection to DP

Figure 7 demonstrates that the advance of the wet region can only be pinned by a directed path of blocked cells that spans the lattice. By *directed* path we mean a connected path of blocked cells that does not turn back. Note that if a path turns back, the part of the path turn-

ing back eventually would become surrounded and hence wet.

Such pinning clusters are branches of a DP cluster, a fact that enables us to map the scaling properties of the pinned interface to the scaling properties of DP clusters [13,14,27]. For a probability of blocked cells smaller than a critical value p_c, the DP clusters are finite. An infinite cluster is present for $p \geq p_c$. For the DPD model we find $p_c \simeq 0.470$, consistent with calculations for DP [55,56]. Near p_c, the size of DP clusters is characterized by a longitudinal (parallel) correlation length $\xi_\parallel$ and a transverse (perpendicular) correlation length $\xi_\perp$ that when $p \to p_c$ diverge as

$$\xi_\parallel \sim |p_c - p|^{-\nu_\parallel}, \qquad \xi_\perp \sim |p_c - p|^{-\nu_\perp}. \tag{3.2}$$

The parallel and the perpendicular correlation length exponents for DP clusters have been calculated [57], with the results

$$\nu_\parallel = 1.733 \pm 0.001, \quad \nu_\perp = 1.097 \pm 0.001 \qquad (d = 1). \tag{3.3}$$

C. Scaling properties

The mapping of the *pinned interface* to DP enables us to estimate the static exponents of this problem from the characteristic exponents of DP clusters. The characteristic length ξ of the pinned regions must be of the order of $\xi_\parallel$, so we can identify the exponent ν to be

$$\nu = \nu_\parallel. \tag{3.4}$$

The global width $W_{\rm sat}$ of the pinned interface should scale as $\xi_\perp$, since its advance is blocked by a DP path. On the other hand, $\xi_\parallel$ must be larger than the system size L for the interface to become pinned, from which follows [13,14,27]

$$W_{\rm sat} \sim \xi_\perp \sim \xi_\parallel^{\nu_\perp/\nu_\parallel} \sim L^{\nu_\perp/\nu_\parallel} \qquad (\xi_\parallel \geq L). \tag{3.5}$$

Comparing with (1.3), we conclude that the roughness exponent is given in terms of the correlation exponents for DP,

$$\alpha = \nu_\perp/\nu_\parallel. \tag{3.6}$$

Substituting (3.3) into (3.6), we predict

$$\alpha = 0.633 \pm 0.001 \qquad (d = 1), \tag{3.7}$$

in good agreement with the experiments and the simulations. For the case $\xi_\parallel \ll L$, we obtain the KPZ result with annealed disorder for length scales ℓ such that $\xi_\parallel \ll \ell \ll L$.

If $p \geq p_c$, the interface becomes pinned after some finite time. However, for $p < p_c$, the DPD model gives rise to an interface that propagates with a constant nonzero velocity. In Sec. I we discussed how near the depinning transition the velocity of the interface scales as a power law. To determine the velocity exponent let us consider the following argument. Near the depinning transition most of the interface is pinned, except for a few regions. The growth occurs by the lateral propagation of the growing regions through the system. The characteristic time required for this propagation is of the order of $t_\times$. During this process the interface advances from one blocking path to the next; the distance advanced is typically of the order of $\xi_\perp \sim W_{\rm sat}$. Using (1.3), (1.4b), (1.7), and (3.2) we obtain

$$v \sim \xi_\perp/t_\times \sim \xi_\parallel^\alpha/\xi_\parallel^z \sim \xi_\parallel^{\alpha-z} \sim f^{-\nu_\parallel(\alpha-z)}. \tag{3.8}$$

Upon comparison with (1.6), we conclude that

$$\theta = \nu_\parallel(z - \alpha). \tag{3.9}$$

This relation can also be derived in a different way [40,41].

Reference [37] showed that for the DPD model, the coefficient λ of the nonlinear term of Eq. (1.8) diverges at the depinning transition

$$\lambda \sim f^{-\phi}. \tag{3.10}$$

The new exponent ϕ can be linked to the other critical exponents that characterize the depinning transition [38]

$$\phi = \nu_\parallel(2 - \alpha - z). \tag{3.11}$$

This prediction is in good agreement with the calculations of Ref. [37] for $d \leq 2$.

The mapping to DP is not unique to the DPD model, but is a general feature of a large class of models [16,27,31,38]. In 1+1 dimensions the agreement between the estimates of the exponents from the mapping to DP and the numerical simulations is quite good.

An interesting problem, still unsolved, is the situation for the moving interface. Measurements of the local width w as a function of the window of observation ℓ lead to an effective exponent $\alpha^m \simeq 0.72$ [15,27]. However, it

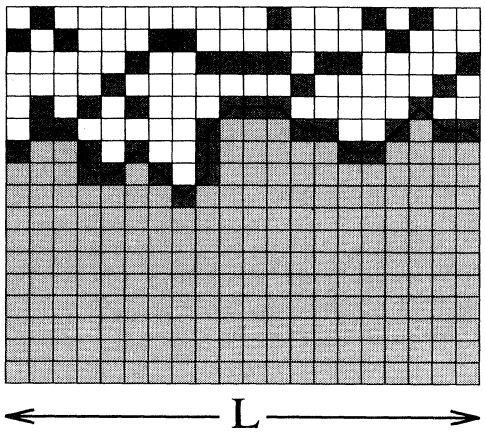

FIG. 7. General conditions for the pinning of the interface. We see in the figure that the path of blocked cells pinning the interface is connected as a DP path, with five possible directions (north, northeast, east, southeast, and south). The shadowing convention for the cells is the same as in Fig. 6.

is possible that the interface in the moving regime might not be self-affine [27].

D. Higher dimensions

In higher dimensions, the mapping to DP is no longer possible since the DP clusters have many holes making it impossible for them to pin the interface. In this case the interface can only be pinned by a DS that is a d-dimensional simply connected hypersurface embedded in a $(d+1)$-dimensional space. The DSs are self-affine and are "directed" in the sense that they do not have overhangs. In $1+1$ dimensions, the DS reduces to DP.

DSs are a new problem about which little is known. Near the critical probability, i.e., the probability for which their size diverges, they can be characterized by two correlation lengths that scale as (3.2). All the relations derived in Sec. III C for the scaling properties of the interface are still valid for higher dimensions, but $\nu_{\|}$ and $\nu_{\perp}$ are now the correlation length exponents for DSs.

We thoroughly studied the DPD models for dimensions up to $6+1$. The results for most of the exponents of interface roughening in disordered media are presented in Table I (see also Fig. 8).

For the case of $2+1$ dimensions, we also calculated the roughness exponent for the moving interface and obtained

$$\alpha^m = 0.52 \pm 0.03 \qquad (d=2), \tag{3.12}$$

in good agreement with the value (2.3) obtained in the experiments.

E. The dynamical exponent z

In the previous subsections we derived scaling relations linking the exponents characterizing the static properties of rough interfaces in the presence of quenched disorder using the mapping of the pinned interface to DP ($d=1$) or DSs ($d>1$). However, the dynamics of the roughening was not derived, leaving us with an unknown exponent z. In this subsection we determine z from the study of how a perturbation, caused by a single unblocked cell, propagates over the interface [58].

To study the propagation of correlations in the system it is better to change the initial conditions in the model and to make the invasion of the cells' nearest neighbors to the wet region in parallel (Fig. 9). If we start the simulation at time $t=0$ with a single unblocked cell in front of the interface we can follow the propagation of correlations simply by monitoring the longitudinal dimension of the invaded region. At each time step, a certain set of cells becomes invaded. In analogy to invasion percolation, we call this set of cells the *percolation shell*. We refer to the longitudinal and the perpendicular components of the average radius of gyration of the percolation shell by $r_{\|}$ and $r_{\perp}$, respectively. From (1.5b) we see that

$$t \sim r_{\|}^{z}. \tag{3.13}$$

For the case $d=1$, all shells are confined between the old directed path that spans the system at $t=0$ and a new pinning path that will block the growth after some time. The region between these two paths is effectively one dimensional, since the vertical distance between them scales as $\xi_{\perp}$, and $\nu_{\perp} < \nu_{\|}$ implies $\xi_{\perp}/\xi_{\|} \to 0$ as $f \to 0$.

For any cell on the interface that becomes wet at time t, we can find the cell from which it was invaded at the previous time step and recreate the sequence of invasion

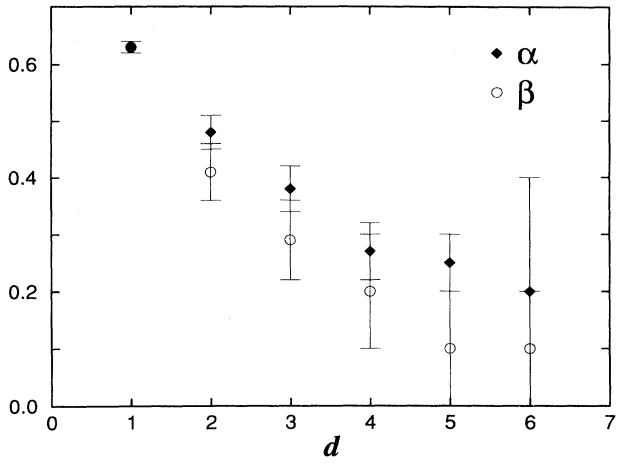

FIG. 8. Values of the exponents α and β, for the DPD model for dimensions up to $6+1$. The results plotted suggest that this class of models has no critical dimension.

TABLE I. Critical exponents of the DPD model for dimensions up to $6+1$ as measured directly from the simulations.

	Dimensions					
Exponents	$1+1$	$2+1$	$3+1$	$4+1$	$5+1$	$6+1$
$\nu_{\|}$	1.73 ± 0.02	1.16 ± 0.05	0.95 ± 0.1	0.66 ± 0.10	0.6 ± 0.1	0.5 ± 0.1
α	0.63 ± 0.01	0.48 ± 0.03	0.38 ± 0.04	0.27 ± 0.05	0.25 ± 0.05	0.2 ± 0.2
z	1.01 ± 0.02	1.15 ± 0.05	1.36 ± 0.05	1.58 ± 0.05	1.7 ± 0.1	1.8 ± 0.2
$\nu_{\perp}$	1.10 ± 0.02	0.57 ± 0.05	0.34 ± 0.05	0.2 ± 0.1	0.15 ± 0.05	0.1 ± 0.1
β	0.63 ± 0.01	0.41 ± 0.05	0.29 ± 0.07	0.2 ± 0.1	0.1 ± 0.1	0.1 ± 0.1
ψ	0.33 ± 0.04	0.59 ± 0.07	0.74 ± 0.09	1.00 ± 0.09		
θ	0.58 ± 0.07	0.8 ± 0.2	1.0 ± 0.2	1.0 ± 0.2		

events that leads from the initial cell to any given cell on the interface (Fig. 10). The trajectory of this sequence follows the upper pinning path and is effectively one dimensional. Its length ℓ scales as its average end-to-end distance $r_{\|}$. On the other hand, ℓ is equal to the time t needed to reach the end of the path. Hence $t \sim r_{\|}$ and from (3.13) we conclude that $z = 1$. This result is supported by our simulations (Table II).

For the case $d > 1$, we must consider the region bounded by two self-affine DSs. This region is effectively d dimensional since $\xi_{\perp}/\xi_{\|} \to 0$. Hence the shortest path leading from the initial point to any point of this region is effectively confined to a d-dimensional hyperplane (Fig. 11). This shortest path has to avoid blocked cells in this hyperplane, *as does* the shortest path of isotropic percolation. For isotropic percolation it is known that the length of the shortest path ℓ scales with the Euclidean end-to-end distance r as $\ell \sim r^{d_{\min}}$ [55]. The similarity between the geometrical properties of the paths in DPD and isotropic percolation leads us to propose

$$z = d_{\min}. \tag{3.14}$$

We are arguing that the invading front moves on a d-dimensional isotropic percolation cluster (see Figs. 10 and 11). The critical threshold is smaller for DPD than in the case of the usual isotropic percolation since (i) some of the blocked cells are eroded and (ii) our systemis a d-dimensional slab. The critical threshold can be determined by the spanning of the invading front in the d-dimensional slab. We confirm that we are at the critical threshold by numerically studying the survival probability of these clusters, as described in [15,16], and verify that we reach the threshold where the invading cluster spans the system.

To test the argument leading to (3.14), we perform simulations for both DPD and percolation for $d = 1$–6. We present our results for both z and $d_{\min}$ in Table II (see also Fig. 12) [59].

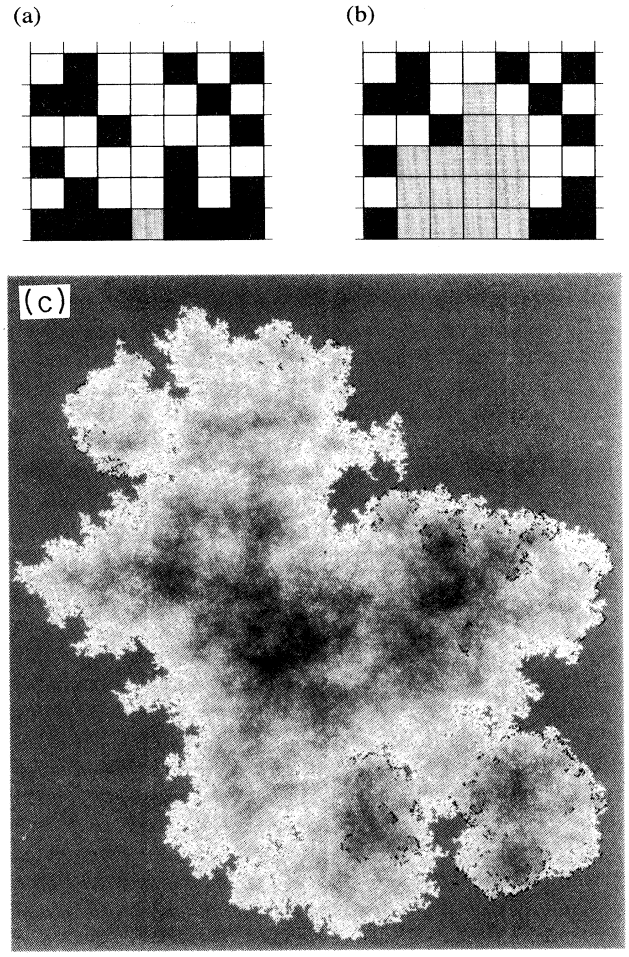

FIG. 9. (a) Initial conditions in the DPD model for the growth of single avalanches: all sites in the bottom edge except one are blocked. The color convention for the cells is the same as in Fig. 6. (b) The wet region after some time; the quantity $n(t)$ defined in the text counts the number of unblocked cells in the interface, in this case 8. (c) Horizontal projection of an avalanche in $2+1$ dimensions for $p \simeq p_c$. The avalanche was started at the center of the figure and is shown at time 2^{10}. The current diameter of the cluster is approximately 2^{10}. The uniform gray area shows the region left dry since the beginning of the process. The darkest shade of gray corresponds to the largest heights of the interface. The black dots, forming a "fractal dust," indicate the unblocked cells at the interface.

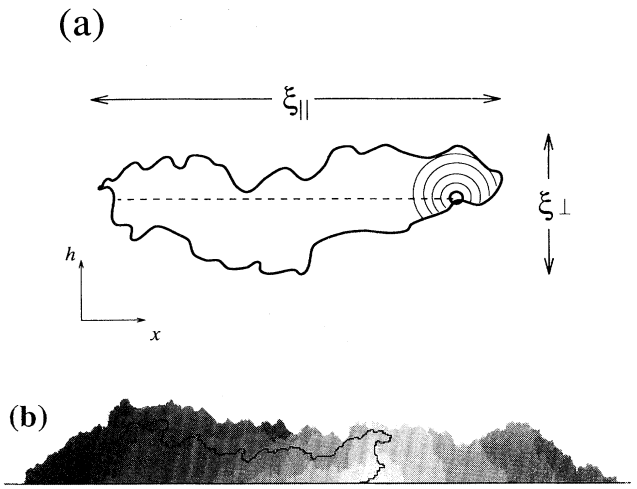

FIG. 10. Illustration of the dynamics of the DPD model for $1 + 1$ dimensions. (a) *Schematic representation* of a region defined by two pinning paths. The heavy circle indicates the origin for the invasion, the thin arcs represent the positions of the invading front at successive times, and the dashed line represents schematically the path for the invasion. (b) *Simulation* results for invasion after 2^{10} time steps starting from a single cell near the center. We show the invaded region at a sequence of times that are multiples of 128. Regions invaded at later times are displayed in darker shades of gray. The path from the origin to the latest invaded point is shown in black. Although this path displays some fluctuations in the vertical direction, they can be disregarded since $\nu_{\|} > \nu_{\perp}$, so as $p \to p_c$, $\xi_{\perp}/\xi_{\|} \to 0$. Thus the distance propagated by the invading front is proportional to time. Since $t_{\times} \sim \ell$, we can conclude that $z = d_{\min} = 1$.

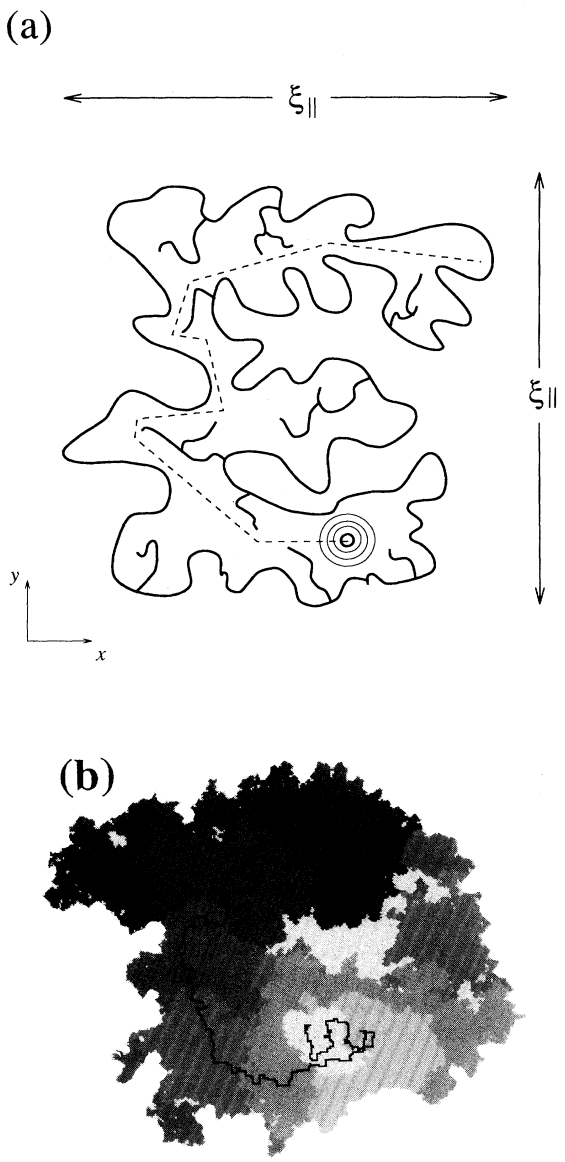

FIG. 11. Illustration of the dynamics of the DPD model for $2+1$ dimensions. (a) *Schematic representation* of the xy projection of the region defined by two pinning self-affine DSs. The heavy circle indicates the origin for the invasion, the thin arcs represent the xy projections of the invading front at successive times, and the dashed line represents schematically the path for the invasion. (b) *Simulation* results for invasion after 2^{10} time steps starting from a single cell located to the left of the center. We show the xy projection of the invaded region at a sequence of times that are multiples of 128. Regions invaded at later times are displayed in darker shades of gray. It is visually apparent that it takes a long time to invade some regions close to the origin because the path to that position (shown in black) appears to be a fractal curve of dimension greater than one. The fluctuations in the vertical direction can be disregarded since we know that $\xi_{\perp}/\xi_{\parallel} \to 0$. We find that the path can be identified with the shortest path (the "chemical distance") of isotropic percolation and that its length scales with the linear distance r to the point as $r^{d_{\min}}$.

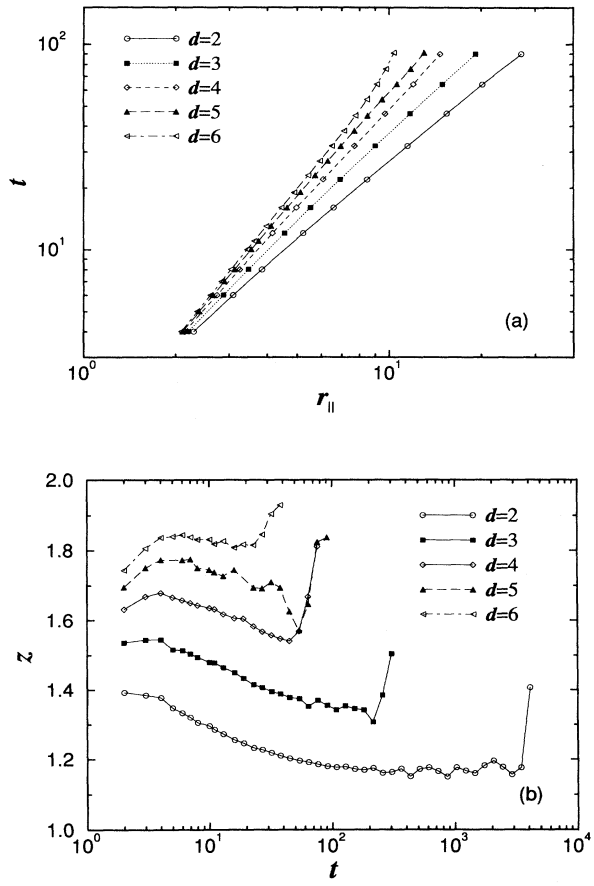

FIG. 12. (a) Scaling with time of the horizontal length of a DPD cluster in $d+1$ dimensions grown from a single cell. Shown is a plot of time t as a function of $r_{\parallel}$, which is the average of the parallel components of the radius of gyration of the shell. The asymptotic slope is z. (b) Consecutive slopes analysis of the data displayed in (a). Note that, after some transient behavior, a transition to a power-law scaling occurs. For higher dimensions, the power-law scaling is affected by finite-size effects for larger times.

It is well known that for isotropic percolation the upper critical dimension is $d_c = 6$, i.e., for $d > d_c$ the mean field result $d_{\min} = 2$ becomes exact [55]. This suggests an upper critical dimension $d_c + 1 = 7$ for the *dynamics* of the DPD models, which are in the universality class of Eq. (1.8), and that $z = 2$ for $d + 1 \geq 7$.

Since the dynamics of Eq. (1.8) and the models in the DPD universality class are connected to isotropic percolation, while the static properties are mapped to DP or DSs, it is possible that the upper critical dimension determined in this study *may be valid only for the dynamics.* It is also possible that d_c for the static properties may not exist, on the basis of the following argument. When, e.g., a one-dimensional object is embedded in a d-dimensional space, we expect that as we increase d, the interactions between the different parts of the object decrease. At a certain $d = d_c$, these interactions can be neglected and the exponents become those of the ideal noninteracting case. In contrast, when the dimension of the object is

TABLE II. Dynamical exponent z for the DPD model in $d+1$ dimensions and the shortest path exponent $d_{\min}$ for isotropic percolation for a d-dimensional cubic lattice of L^d sites. The values indicated by an asterisk are exact, while the remaining values were calculated in our simulations by studying the consecutive slopes of the linear regime in Fig. 12. At the critical dimension $d_c = 6$, one should not expect to find the exact result $d_{\min} = 2$ because logarithmic corrections are generally present. The system sizes used in the simulations range from $L = 4096$ for $d = 2$ to $L = 16$ for $d = 6$. Each result is averaged over 10^6–10^7 realizations of the disorder.

	DPD		Percolation	
d	p_c	z	p_c	$d_{\min}$
1	0.4698 ± 0.0005	1.01 ± 0.02	1^*	1^*
2	0.7425 ± 0.0005	1.15 ± 0.05	0.5927 ± 0.0005	1.13 ± 0.03
3	0.8425 ± 0.0005	1.36 ± 0.05	0.3116 ± 0.0005	1.38 ± 0.02
4	0.8895 ± 0.0005	1.58 ± 0.05	0.197 ± 0.005	1.53 ± 0.05
5	0.9175 ± 0.0005	1.7 ± 0.1	0.141 ± 0.005	1.7 ± 0.1
6	0.931 ± 0.005	1.8 ± 0.2	0.107 ± 0.005	1.8 ± 0.2

not fixed but increases with d, as in the case of DSs in which the object is one dimension smaller than the space, we expect to move away from the noninteracting limit. In fact, the analytical solution of the DPD model in the Cayley tree suggests that the upper critical dimension for the *statics* might be ∞ [16].

Thus we see that the DPD model has three *independent* exponents ν, α and z. The static exponents, ν and α, can be evaluated from the exponents of DP ($d = 1$) or DSs ($d > 1$). On the other hand, the dynamics of the model is related to isotropic percolation in d dimensions. We find that z is equal to the exponent $d_{\min}$ characterizing the scaling of the shortest path in isotropic percolation. The model also allows us to calculate the roughness exponents determined in the experiments for both the pinned and the moving interfaces. However, at this time, no explanation is available for why α changes value at the transition or for the value of α^m.

IV. THE AVALANCHE MECHANISM OF INTERFACE MOTION

The study of the scaling properties of self-organized systems is of great importance for many fields [44–51]. In this section we show how avalanches can be generated in the DPD model and we study their properties. We then relate those avalanches to the SOD variant and discuss some of the results that have been obtained recently for the SOD model and compare them with our numerical results.

A. Avalanches in the DPD model

As we discussed above, for $p > p_c$ the growth of the interface for the DPD model is stopped by the spanning path of a DP cluster in 1+1 dimensions or a spanning self-affine DS in $(d+1)$ dimensions. Even when the growth is completely stopped, the blocked cells on the interface may still erode, but at an *infinitesimal* rate. With this assumption, we can remove a blocked cell at random when the interface is completely stopped, thereby producing an avalanche that eventually will die out when the front reaches a second pinning hypersurface (Fig. 13).

An alternative way of producing avalanches is to start the growth from a single wet cell in a row of blocked cells at time $t = 0$ (Fig. 9). For $p > p_c$, the growing clusters will eventually become pinned by a blocking path. Below p_c most clusters will grow indefinitely, although some might become pinned by the blocking surfaces.

In analogy with conventional percolation, the survival probability $P_{\rm surv}(t)$ of the clusters will decay as a power law [60]

$$P_{\rm surv}(t) \sim t^{-\tau_{\rm surv}} \qquad (t \ll t_\times), \tag{4.1}$$

where $t_\times \sim \xi_\parallel^z$. In Fig. 14 we show the scaling of $P_{\rm surv}(t)$ for $2+1$ dimensions, and the value of $\tau_{\rm surv}$ is given in Table III.

If $p > p_c$, $P_{\rm surv}(t \gg t_\times)$ approaches zero exponentially. If $p < p_c$, $P_{\rm surv}(t \gg t_\times)$ approaches a constant value $P_{\rm surv}(\infty)$, the probability of an infinite cluster. Thus studying $P_{\rm surv}(t)$ provides a very accurate method of estimating p_c. We calculated $P_{\rm surv}(t)$ and determined both the exponent $\tau_{\rm surv}$ and p_c for $d = 1 - 6$ (Table III). Using these high-accuracy determinations of the critical probability p_c we were able to measure with higher precision the other critical exponents (Appendix A and Tables I and III).

The probability distribution of avalanches of "volume" s, $P_{\rm aval}(s)$, is calculated as the ratio of the number of avalanches of volume s to the total number of avalanches. We find [15]

$$P_{\rm aval}(s) \sim s^{-\tau_{\rm aval}} f_3(s/s_0), \tag{4.2}$$

where s is the number of cells invaded during an avalanche, $s_0 \sim \xi_\perp \xi_\parallel^d$ is the characteristic volume of an avalanche, and $f_3(u)$ is a scaling function that approaches a constant for $u \ll 1$ and decays exponentially for $u \gg 1$ (Fig. 15).

The exponents $\tau_{\rm surv}$ and $\tau_{\rm aval}$ can be related as

$$s \sim r_\perp^d \, r_\parallel^d \sim r_\parallel^{d+\alpha} \sim t^{(d+\alpha)/z}. \tag{4.3}$$

On the other hand, $P_{\rm aval}(s)ds = P_{\rm surv}(t)dt$. Hence from (4.1) and (4.3) follows

$$t^{-\tau_{\rm aval}(d+\alpha)/z} \, t^{(d+\alpha)/z-1} \, dt = t^{-\tau_{\rm surv}} \, dt. \tag{4.4}$$

From (4.4), we find

$$\tau_{\rm aval} = 1 + \frac{z(\tau_{\rm surv} - 1)}{d+\alpha}. \tag{4.5}$$

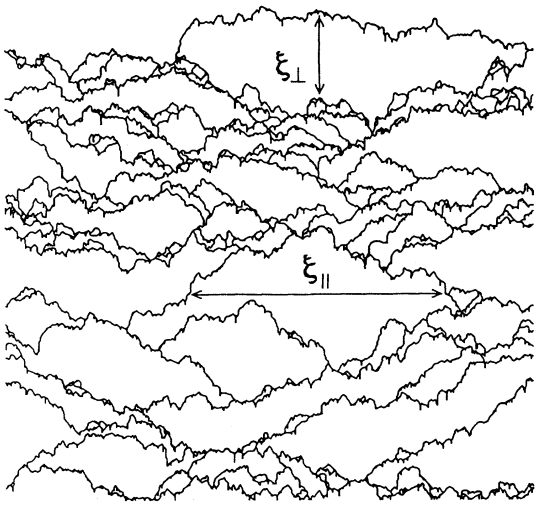

FIG. 13. Successive series of pinned interfaces for the DP model with $L = 400$ and $p = 0.5 > p_c$. We show the boundaries of avalanches, produced by removing a randomly chosen blocked cell from the previously pinned interface. The correlation lengths $\xi_\parallel$ and $\xi_\perp$ displayed describe the typical size of the avalanches.

If $p = p_c$, the dynamical critical exponents β and z can be obtained from the dependence of the avalanche volume s on time. We can define a new exponent δ that characterizes the time dependence of the number of *unblocked cells* in the interface, i.e., the size of the percolation shell (Fig. 9)

$$n(t) \sim t^\delta. \tag{4.6}$$

To relate the new exponent δ to z and α, we start by noticing that the size of the invaded region scales as

$$s \sim r_\parallel^{d+\alpha} \sim \int_0^{r_\parallel^z} n(t)dt \sim r_\parallel^{z(\delta+1)}. \tag{4.7}$$

From (4.7), we obtain

$$\delta = \frac{d+\alpha}{z} - 1. \tag{4.8}$$

In $1+1$ dimensions, $z = 1$, so $\delta = \alpha = \beta$, which agrees with the simple geometrical picture that the projection of the growing region scales as the length of the steepest moving terrace, which scales as the width of the whole system $W(t) \sim t^\beta$. In $1+1$ dimensions, we find $\delta = 0.60 \pm 0.03$, in agreement with the above relations.

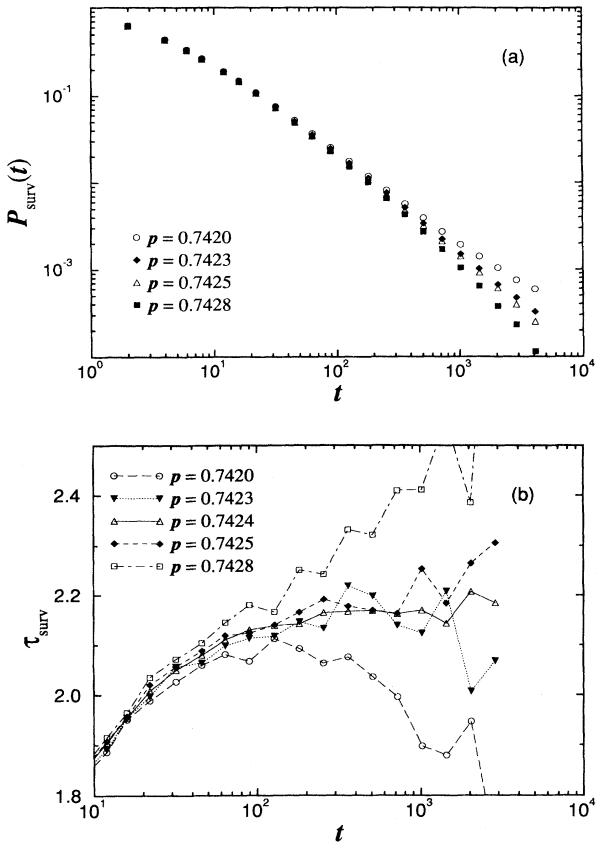

FIG. 14. Distribution of survival times for avalanches $P_{surv}(t)$ for $2+1$ dimensions. The system size is 2048 and 10^6 avalanches were produced for each probability. In (a) we show data for several probabilities close to the critical value. The straight part of the distribution can be well fitted to a power law with exponent 2.18. In (b) we show the consecutive slopes of the data in (a). The figure makes clear that we can predict with great precision the value of p_c and the error of the estimate.

The projection of the shell of unblocked cells in the interface forms a *fractal dust* (Fig. 9). The fractal dimension of this dust d_{dust} can be related to τ_{surv} [16]. The fractal dimension of the dust must be the same as the fractal dimension of the "bubbles" surrounding the regions of space confined by two DSs. The distribution of

TABLE III. Critical exponents for the avalanches in the DPD model for dimensions up to $6+1$ as measured directly from the simulations. For comparison we also show the estimates obtained with (4.17) and (4.18).

	Dimensions					
Exponents	$1+1$	$2+1$	$3+1$	$4+1$	$5+1$	$6+1$
γ_p	1.98 ± 0.03	1.41 ± 0.05	0.95 ± 0.05	0.8 ± 0.2	0.5 ± 0.2	0.3 ± 0.2
δ	0.60 ± 0.03	1.14 ± 0.06	1.6 ± 0.1	1.9 ± 0.2	2.1 ± 0.2	2.5 ± 0.3
τ_{surv}	1.46 ± 0.02	2.18 ± 0.03	2.54 ± 0.05	3.0 ± 0.2		
τ_{aval}	1.26 ± 0.02	1.51 ± 0.07	1.70 ± 0.05	1.7 ± 0.1	1.8 ± 0.1	1.9 ± 0.1
τ_{aval}^{MP}	1.3 ± 0.1	1.5 ± 0.1	1.6 ± 0.2	1.6 ± 0.2	1.6 ± 0.1	1.6 ± 0.1
τ_{aval}^{OPZ}	1.2 ± 0.1	1.2 ± 0.1	1.2 ± 0.1	1.2 ± 0.1	1.1 ± 0.1	1.1 ± 0.1

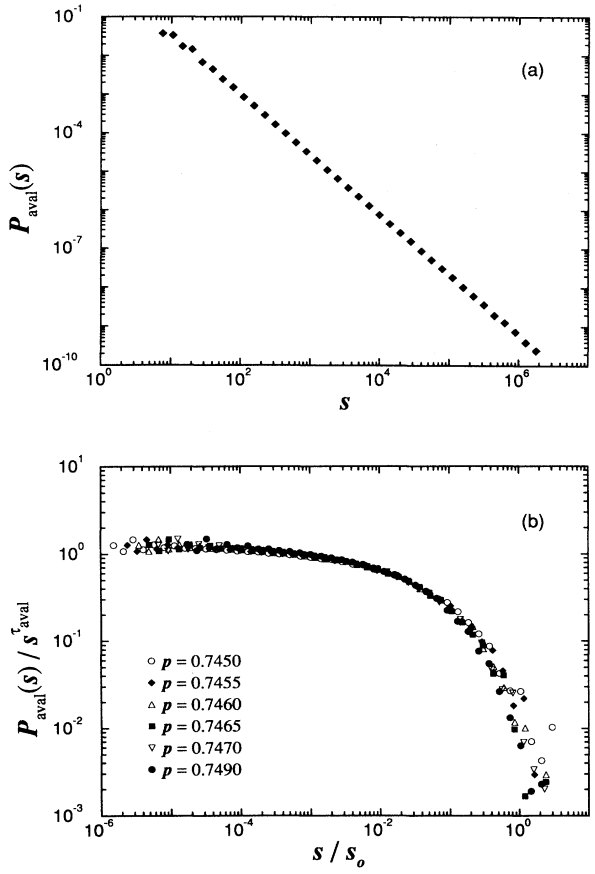

FIG. 15. Distribution of avalanches size P_{aval} for $2+1$ dimensions. The system size is 2048 and 10^6 avalanches were produced for each probability. In (a) we show the data for the critical probability; a good power-law fit can be done with an exponent 1.51. (b) shows a data collapse, according to (4.2), for several distinct probabilities close to p_c.

these confined regions can be linked to the distribution of survival times for the avalanches. Thus we have

$$P_{\text{aval}}(r_{\parallel})\, dr_{\parallel} = P_{\text{surv}}(t)\, dt \tag{4.9a}$$

and

$$r_{\parallel}^{-\tau_{\parallel}}\, dr_{\parallel} = t^{-\tau_{\text{surv}}}\, dt. \tag{4.9b}$$

Since $t \sim r_{\parallel}^{z}$, it follows that

$$\tau_{\parallel} - 1 = z(\tau_{\text{surv}} - 1). \tag{4.10}$$

On the other hand, it is well known that the fractal dimension of some dust separated by regions whose size follows a power-law distribution $P_{\text{aval}}(r_{\parallel}) \sim r_{\parallel}^{-\tau_{\parallel}}$ is given by

$$d_{\text{dust}} = \tau_{\parallel} - 1, \tag{4.11}$$

leading to

$$d_{\text{dust}} = z(\tau_{\text{surv}} - 1). \tag{4.12}$$

Since $d_{\text{dust}} < \delta$, the fractal dust is packed in "moving blocks." These moving blocks behave like quasiparticles, which are distributed in a fractal way with dimension d_{dust}. This description is supported by numerical studies of the correlation function of the dust.

We can also relate the velocity of the interface to the number of unblocked cells in the interface, as defined in (4.6). The velocity at each instant can be obtained as the number of unblocked cells divided by the size of the parallel projection of the invaded region

$$v \sim n(t)/\xi_{\parallel}^{d} \sim t^{\delta}/\xi_{\parallel}^{d} \sim \xi_{\parallel}^{z\delta-d} \sim f^{-\nu_{\parallel}(z\delta-d)}. \tag{4.13}$$

Comparing with (1.6), we obtain

$$\theta = \nu_{\parallel}(d - z\delta). \tag{4.14}$$

As a consistency check, we note that (4.14) can also be obtained by equating (4.8) with (3.9).

We measured the components of the radius of gyration of the avalanches in the longitudinal and transverse directions for both 1+1 and 2+1 dimensions (Fig. 16). For 1+1 dimensions we find, for a system of size $L = 131\,072$,

$$\nu_{\parallel}^{\text{aval}} = 1.73 \pm 0.02, \qquad \nu_{\perp}^{\text{aval}} = 1.10 \pm 0.02 \qquad (d = 1), \tag{4.15}$$

in good agreement with the correlation length exponents of DP given in Eq. (3.3).

For the case of 2+1 dimensions, we find the correlation length exponents to be

$$\nu_{\parallel}^{\text{aval}} = 1.16 \pm 0.05, \qquad \nu_{\perp}^{\text{aval}} = 0.57 \pm 0.05 \qquad (d = 2), \tag{4.16}$$

for a system of linear size $L = 2048$. The estimates (4.16) predict, from (3.6), that $\alpha = 0.49 \pm 0.1$, in good agreement with the value obtained from the analysis of the scaling of the width (see Table I).

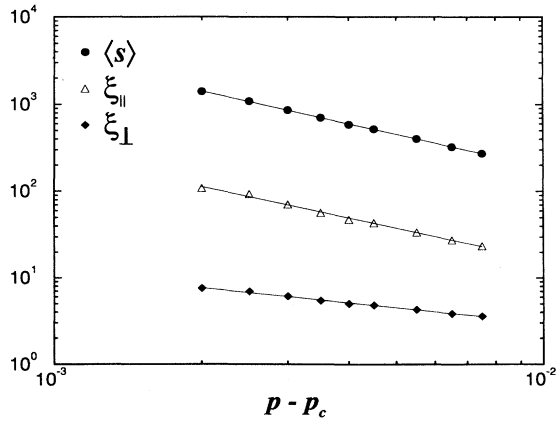

FIG. 16. Scaling of the average size s and parallel and perpendicular correlation lengths of the avalanches for $2+1$ dimensions. These quantities were calculated according to the method described in Appendix A. Good power-law fitting was found with the exponents given in (4.16).

B. Avalanches in the SOD model

A variant of the model discussed so far, in which the growth is made in an invasion percolation fashion, was introduced in Ref. [13]. Subsequently, a similar model was introduced in Ref. [43] and studied in detail in Refs. [44–47]. The SOD model can still be mapped to DP. In fact, the SOD model is always at the depinning transition.

For the SOD model, the cells are not labeled blocked or unblocked. Instead, we keep in memory the pinning forces at each cell. The growth proceeds by the invasion (wetting) of the cell that is a nearest neighbor to the wet region and has the weakest noise, i.e., with the smallest random number η. Then we erode any overhangs that might have been formed, i.e., we wet any dry cell below a wet cell. The unit time is defined as the volume of the invaded region, i.e., it takes one time unit to invade one cell.

With the time defined in this way, many authors [13,43–47] then define a dynamical exponent $z_{\rm SOD}$. By a simple argument, we can relate $z_{\rm SOD}$ with the dynamical exponent z, discussed in Sec. III for the DPD model. In the SOD model the time is defined as

$$t_{\rm SOD} \sim \int_0^t n(t')dt' \sim \int_0^t t'^{\delta} dt' \sim t^{\delta+1}.$$

Here, $n(t)$ is the number of unblocked active cells as defined in Eq. (4.6). Using Eq. (4.8), we obtain the relation

$$z_{\rm SOD} = z(\delta + 1),$$

in good agreement with the numerical value $z_{\rm SOD} \simeq 1.63$ found in [45].

At any given instant t, the interface is characterized by a set of noises $\{\eta\}$. The smallest of these, denoted $\eta_{\rm min}(t)$, is useful in characterizing the state of the system at that instant. Reference [45] argued that every possible configuration of the interface corresponds to a path on a cluster of sites with values of the noise greater than or equal to $\eta_{\rm min}$. This fact and the mapping to DP imply that $\eta_{\rm min}(t)$ cannot exceed $q_c \equiv 1 - p_c$ since that would imply the existence of a directed path of blocked cells spanning the system for a probability smaller than p_c.

The general tendency is for $\eta_{\rm min}(t)$ to increase, until it reaches q_c, but its growth is not monotonic (Fig. 17). When we start the growth from a flat interface the noise has a uniform distribution between 0 and 1. This implies that $\eta_{\rm min}(1)$ will be very close to zero. The interface will then advance to a new position and the noise $\eta_{\rm min}(1)$ will be replaced by a new noise. Since $\eta_{\rm min}(1)$ is very small then it is very likely than the new noise will be larger than $\eta_{\rm min}(1)$. So we see that $\eta_{\rm min}(2) > \eta_{\rm min}(1)$ with high probability.

Initially, $\eta_{\rm min}(t)$ will grow monotonically. However, at some time t_0 all cells in the interface with small noise will have been eroded, so the probability that $\eta_{\rm min}(t_0+1) < \eta_{\rm min}(t_0)$ will no longer be irrelevant. Hence $\eta_{\rm min}(t)$ can decrease. During some time interval Δt, $\eta_{\rm min}(t)$ will be smaller than $\eta_{\rm min}(t_0)$, which can only occur in a connected region since all other cells in the interface have larger noise values. Therefore we can identify the avalanches with the regions invaded during the time interval from t_0 to $(t_0 + \Delta t)$ [47].

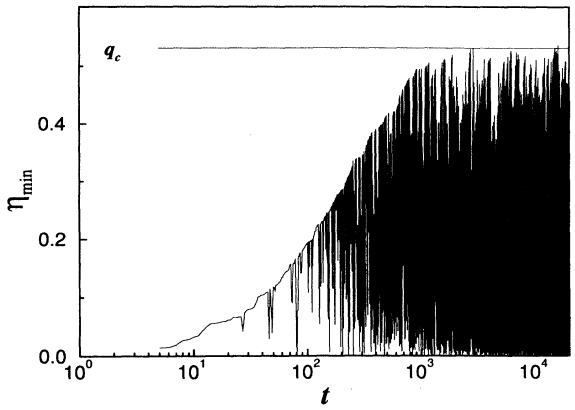

FIG. 17. Evolution with time of $\eta_{\rm min}$. Every local maximum defines the end of an avalanche and the beginning of another. Regions with monotonic growth indicate that the avalanches have size 1. After the transient period, the critical state is reached and the maxima become equal to $q_c = 1 - p_c$.

A different regime is reached when $\eta_{\rm min}(t)$ reaches the value q_c, for an infinite system (for a finite system there will be fluctuations around this value). Then the interface is just at a DP path that spans the system. This implies that for some time steps the advance will be accomplished by invading cells with $\eta_{\rm min} < q_c$, until a new DP path is found, for which $\eta_{\rm min}$ is again equal to q_c.

The early stage in which $\eta_{\rm min}$ is smaller than q_c is referred to as the *transient* regime; after it ends, the system is said to be in the *critical* state. From then on, the interface will advance between spanning paths of the DP cluster. So we see that the avalanche picture for the SOD model is similar, *after* the transient regime, to the avalanche image of the DPD model in which we unblock a site at random. This argument is supported by numerical results [15,16,44–47].

The problem with the previous definition of avalanches is that it is precise only for the critical state. To remedy this situation, Ref. [47] introduced a modified definition, in which avalanches for $q < q_c$ are finished whenever $\eta_{\rm min}$ passes the threshold q.

A different method to define avalanches for $q < q_c$ was proposed in Refs. [15,16], whereby the growth is allowed only until the first time the system has $\eta_{\rm min} = q$. In spite of the different definitions and initial conditions, numerical calculations reveal that both approaches lead to identical exponents, at least for $d \leq 2$.

Theoretical predictions for the avalanche size distribution were made in Refs. [44–47]. We extend an argument proposed by Olami-Procaccia-Zeitak (OPZ) for $1+1$ dimensions [46], to higher dimensions, obtaining

$$\tau_{\rm aval}^{\rm OPZ} = \frac{d+1}{d+\alpha}. \tag{4.17}$$

On the other hand, Maslov and Paczuski (MP) [47] predict

$$\tau_{\rm aval}^{\rm MP} = 1 + \frac{d - 1/\nu_{\|}}{d + \alpha}. \tag{4.18}$$

Our simulations enable us to test the accuracy of both of these formulas (Table III). The OPZ relation (4.17) cannot be correct for all d: For $d = 1$, $\tau_{\rm aval}^{\rm OPZ}$ is slightly below numerical results, but for $d > 1$, (4.17) decreases while $\tau_{\rm aval}$ increases. On the other hand, the MP relation (4.18) predicts values consistent with our simulations. Moreover, recent work on the Cayley tree [61] suggests that the upper critical dimensions for this class of models should be $d_c = \infty$ and that $\tau_{\rm aval}(d = \infty) = 2$, again in good agreement with (4.18). Those calculations also lead to the estimates $\alpha = 0$, $\beta = 0$, $\nu_{\perp} = 0$, and $\nu_{\|} = 1/4$.

However, from the MP relation (4.18), we can derive (see Appendix A)

$$\gamma_p^{\rm MP} = 1 + \nu_{\perp}, \tag{4.19}$$

where γ_p is the percolation exponent characterizing the divergence of the average volume of the clusters at the transition. In Table III we show the values obtained for γ_p in our simulations. We can see that several values are smaller than one, while (4.19) predicts $\gamma_p \geq 1$ for all d.

A limitation of the SOD model is that the velocity of the interface is constant, thereby making the "temporal" definition of avalanches ambiguous, since our "physical sense" of an avalanche is the very fast invasion of a certain region while here everything happens at constant velocity [62]. To avoid this "paradox," a different time unit can be defined in which the time required to invade a cell would depend exponentially on the value of $\eta_{\rm min}$. We define this dependence as

$$t \sim \exp\left(\frac{\eta_{\rm min}}{\eta_0}\right), \tag{4.20}$$

where η_0 is some constant much smaller than 1.

V. THE GRADIENT DPD MODEL

The DPD model can predict the roughness exponent obtained in the experiments, but several other experimental findings are not explained. One problem is how to explain that in the experiments the driving force, at some stage, takes its critical value, allowing the interface to become pinned. Also, the effect of evaporation on both the saturation width $W_{\rm sat}$ and the average height h_c of the pinned interface cannot be explained by the DPD model. In order to try to quantify these ideas, we propose and study in this section an extension to the DPD model that takes into account these effects.

A. Motivation and definition

We anticipate, on physical grounds, that the smaller the evaporation rate [64], the larger the critical height. To test this hypothesis we repeated our imbibition experiments in different conditions of evaporation. We find that as we decreased the evaporation rate, the height reached by the interface indeed increased (Fig. 2).

The basic idea is that the driving force is no longer a constant, but rather it depends on the height, so $F = F(h)$. This implies that the density of blocked cells will also be a function of the height, so $p = p(h)$.

In $1 + 1$ dimensions, we model the pinning obstacles by randomly "blocking," in a lattice of horizontal size L, a fraction $p(h)$ of the cells in each horizontal row, where h is the height from the bottom of the lattice and $p(h)$ is a monotonically increasing function of h. The original DPD model corresponds to the case $p(h)$ =const.

This extension of the model can be justified on physical grounds. In fact, we know that the actual disorder in the paper is *not height dependent*; however, its *effect* in pinning the propagation of the fluid is *increasing with height*, due to the decrease in the fluid pressure. The most physical assumption is an exponential decrease of the fluid pressure or, equivalently, of the driving force. This will lead to an "effective" increase in the density of pinning obstacles [65] as we depart from the reservoir. Hence

$$p(h) - p_0 \propto 1 - e^{-h/h_0}. \tag{5.1}$$

If $h \ll h_0$ (and $p_c - p_0 \ll p_c$), we can write

$$p(h) - p_0 \propto h_0^{-1} h \propto gh. \tag{5.2}$$

Hence, in this limit, we find a constant *nonzero* gradient g in the density of pinning obstacles.

The gradient in our model is intended to reproduce the combined effect on the driving force of all the factors referred to in Sec. IV: decrease of fluid density because of evaporation, changes in the density of the suspension, etc.

B. Simulations

The presence of the gradient g changes the width of the pinned interface and its scaling form. Our simulations show that for observation scales ℓ much smaller than some characteristic crossover length $\ell'_{\times}$, the saturated width behaves as $w \sim \ell^{\alpha}$, but for $\ell \gg \ell'_{\times}$, the width saturates at a value $W_{\rm sat}$ that depends upon the gradient as

$$W_{\rm sat} \sim g^{-\gamma} \qquad (\ell \gg \ell'_{\times}). \tag{5.3}$$

This behavior can be expressed by a scaling law of the form

$$w(\ell, g) \sim \ell^{\alpha}\, f_4(\ell/\ell'_{\times}), \tag{5.4a}$$

where

$$\ell'_{\times} \sim g^{-\gamma/\alpha}. \tag{5.4b}$$

The scaling function $f_4(u)$ satisfies $f_4(u \ll 1) \sim$const and $f_4(u \gg 1) \sim u^{-\alpha}$. Our simulations for a system of size $L = 16\,384$ yield the exponents

$$\alpha_{\rm sim} = 0.63 \pm 0.02, \quad \gamma_{\rm sim} = 0.52 \pm 0.02 \qquad (d = 1). \tag{5.5}$$

We stress that the validity of the scaling law (5.4b) and the values of the exponents do not depend on the exact form of $p(h)$, but only on the value of $\nabla p(h)$ at h_c [66].

The exponent γ can be related to $\nu_\perp$. A point of the interface, at a distance $W_{\rm sat}$ away from the critical height, is pinned by a DP path if the transverse size of that cluster is of order $\xi_\perp(p)$. At that point we have $p = p(h_c \pm W_{\rm sat}) \approx p_c \pm gW_{\rm sat}$. Therefore, using Eq. (3.2) we find [66–69]

$$W_{\rm sat} \sim \xi_\perp(p) \sim |p_c - (p_c \pm gW_{\rm sat})|^{-\nu_\perp} \tag{5.6}$$

and

$$W_{\rm sat} \sim |gW_{\rm sat}|^{-\nu_\perp}. \tag{5.7}$$

From (5.3) and (5.7) follows

$$\gamma = \nu_\perp/(1+\nu_\perp). \tag{5.8}$$

Since $\nu_\perp$ is known accurately, Eq. (5.8) predicts

$$\gamma = 0.523 \pm 0.001 \qquad (d=1), \tag{5.9}$$

in good agreement with our simulation result (5.5).

The generalization of the model, with the gradient, to $2+1$ dimensions is straightforward. We simulated the model for a 512×512 system; the critical exponents that give the best data collapse are (see Fig. 18)

$$\alpha_{\rm sim} = 0.43 \pm 0.04, \quad \gamma_{\rm sim} = 0.32 \pm 0.02 \qquad (d=2). \tag{5.10}$$

From these results, we calculate the exponents characterizing the parallel and the perpendicular correlation lengths for the DS problem in $2+1$ dimensions, obtaining

$$\nu_\parallel = 1.1 \pm 0.1, \quad \nu_\perp = 0.47 \pm 0.04 \qquad (d=2). \tag{5.11}$$

These results are in reasonable agreement with calculations of the exponents from the scaling properties of avalanches (see Sec. IV).

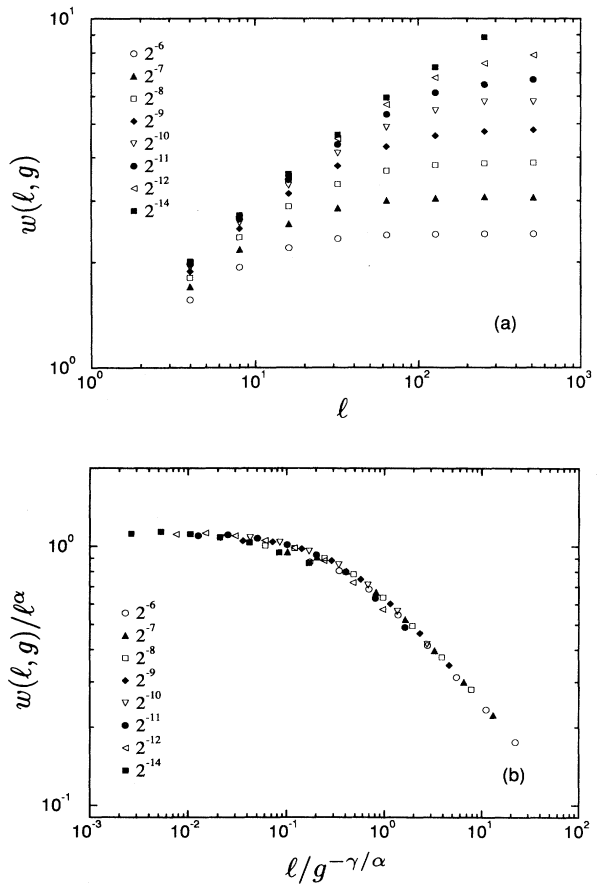

FIG. 18. Simulation results for the width $w(\ell, g)$ of the pinned interface in $2+1$ dimensions, where g is the gradient in the density of blocked cells. (a) The widths for several values of the gradient (averaged over 128 runs for each value of the gradient). (b) The same simulation results, plotted in the scaling form of Eq. (5.4), using the values of the exponents from (5.10).

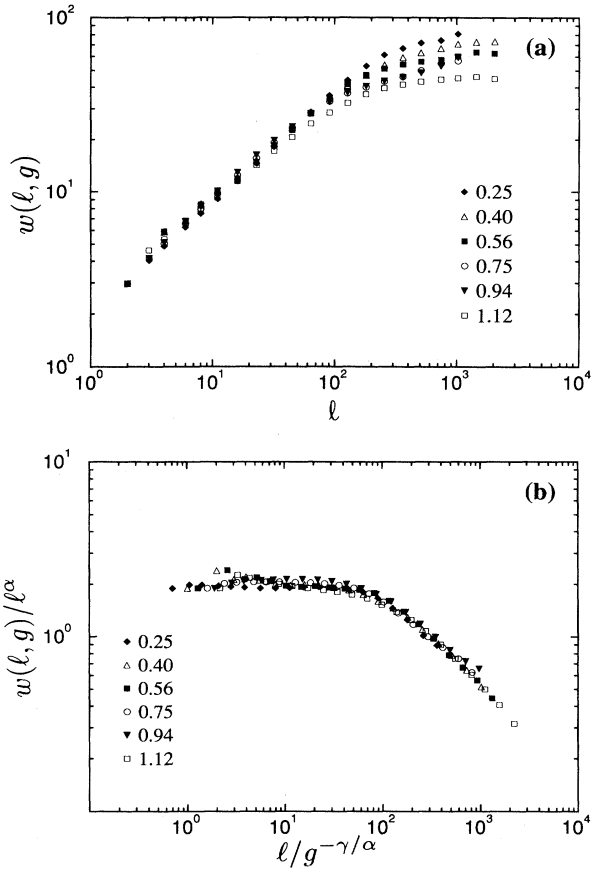

FIG. 19. Experimental results for the width $w(\ell, g)$ of the pinned interface. (a) The widths for several values of the gradient g (in units of g_0). The values of g were calculated as described in the text; the error in these values is smaller than 10%. The widths were corrected by a multiplicative factor to make them coincide for the smallest ℓ. (b) The same experimental results, plotted in the scaling form of Eq. (5.4), using the values of the exponents from (5.13).

TABLE IV. Critical exponents of the gradient DPD model.

	Dimensions	
Exponents	$1+1$	$2+1$
α	0.63 ± 0.02	0.43 ± 0.04
γ	0.52 ± 0.02	0.32 ± 0.02
$\nu_\perp$	1.09 ± 0.08	0.47 ± 0.04
$\nu_\parallel$	1.7 ± 0.1	1.1 ± 0.1

C. Experiments

Without the gradient, the interface has critical behavior only if we tune p_0 to p_c. However, with the gradient the interface always stops at the critical height h_c. This critical height can be calculated from the condition $p(h_c) = p_c$. From (5.2) we obtain

$$h_c \sim g^{-1}, \tag{5.12}$$

i.e., the height reached by the wetting fluid is inversely proportional to the gradient in the disorder.

The experimental data presented in Fig. 19 remarkably resemble the data obtained from the model. However, without knowing the actual value of the gradient in the experiments, it is not possible to check the validity of the scaling law (5.4b) experimentally. Nonetheless, measuring the critical height in the experiments and using Eq. (5.12), we are able to estimate g, the gradient in the "effective disorder," for the experiments, up to a multiplicative constant g_0. Using these experimentally determined values of g, we rescale the results obtained for the width according to the scaling law (5.4b). In Fig. 19 we show this rescaling, where we used

$$\alpha_{\text{expt}} = 0.65 \pm 0.05, \quad \gamma_{\text{expt}} = 0.49 \pm 0.05 \qquad (d = 1). \tag{5.13}$$

The experimental values of both exponents agree well with the results obtained from the simulations (Table IV) and with the theoretical predictions based in the known results from DP.

In summary, in this section we discussed a variant of the DPD model that incorporates evaporation by introducing a gradient in the density of pinning cells [65]. The model provides insight into three previously unexplained aspects of imbibition experiments.

(i) The interface always stops growing after some finite time. Due to the gradient, the wetting interface only moves until it reaches a critical density of pinning cells. This gradient in pinning cells arises from the balance between the evaporation of the fluid and the surface tension, on the one hand, and the capillary forces tending to move it along the paper, on the other.

(ii) The final height of the interface h_c increases when the evaporation is reduced, due to the smaller *effective* gradient in the pinning disorder.

(iii) An exponent γ was found characterizing the dependence on the gradient of the saturation width and the characteristic length $\ell_\times$. Good agreement was found between experimental, theoretical, and numerical calculations of the exponents.

VI. SUMMARY

In this work we introduced and discussed a set of imbibition experiments that probe the behavior of rough interfaces in disordered media. We developed a discrete model, the DPD model, and showed that it correctly predicts the experimental results.

We presented a discussion of the properties of the DPD model, which has been shown in Ref. [37] to be in the same universality class as a continuum differential equation of the KPZ type with quenched disorder. We showed that the model has only three independent exponents — $\nu_\parallel$, α, and z — from which all others can be derived through scaling laws. The mapping to DP enables us to obtain $\nu_\parallel$ and α from the exponents of DP ($d = 1$) or DSs ($d > 1$). On the other hand, a mapping of the dynamics of the DPD model to *isotropic* percolation allow us to determine z.

We introduced avalanches in the DPD model and studied their scaling properties. We then related the avalanches in the DPD model to the avalanches in the SOD variant of the DPD model. We derived scaling laws relating the critical exponents for the avalanches τ_{aval} and τ_{surv} to the other critical exponents of the DPD model, confirming that they are not independent.

Finally, we performed a set of imbibition experiments to study the effect of evaporation on interfacial phenomena. We modify the DPD model to take these effects into consideration and use the present model to predict the experimental results. Again the mapping to DP enables us to estimate the values of the exponents. Good agreement was obtained between experimental, theoretical, and numerical calculations.

ACKNOWLEDGMENTS

We thank I. S. Buldyrev, V. Buldyrev, R. Cuerno, J. Kertész, K. B. Lauritsen, H. Makse, S. Schwarzer, M. Ukleja, T. Vicsek, and P.-z. Wong for valuable contributions and discussions. L.A.N.A. acknowledges financial support from Junta Nacional de Investigação Científica e Tecnológica. S.H. acknowledges partial support from the Bi-National U.S.-Israel Foundation and the Minerva Center for Mesoscopic Physics, Fractals and Neural Networks. The Center for Polymer Studies is supported by the National Science Foundation.

APPENDIX A: CALCULATING THE CORRELATION LENGTH EXPONENTS

In this appendix we discuss the relation between percolation and the growth of clusters by avalanches and use the insight gained to determine the exponents characterizing the divergence of the parallel and perpendicular correlation lengths. As discussed above, the characteristic volume of the avalanches diverges when $p \to p_c$,

$$s_0 \sim (p_c - p)^{-1/\sigma}, \tag{A1}$$

where here [55,56]

$$1/\sigma = d\nu_{\parallel} + \nu_{\perp}. \tag{A2}$$

The average cluster size also diverges for the critical probability

$$\langle s \rangle \equiv \int P_{\rm aval}(s) ds \sim (p_c - p)^{-\gamma_p}, \tag{A3}$$

where

$$\gamma_p = \frac{2 - \tau_{\rm aval}}{\sigma}. \tag{A4}$$

In percolation theory [55,56] this exponent is called γ. To avoid confusion with the growth exponent β, we denote the exponent characterizing the mass of the infinite cluster as β_p, where

$$\beta_p = 1/\sigma - \gamma_p. \tag{A5}$$

We calculated both $\tau_{\rm aval}$ and σ from the scaling of $P_{\rm aval}(s)$ for $d = 1, 2$. We obtained [15,16]

$$\tau_{\rm aval} = 1.26 \pm 0.02, \quad 1/\sigma = 2.8 \pm 0.1 \qquad (d = 1) \tag{A6a}$$

and

$$\tau_{\rm aval} = 1.51 \pm 0.07, \quad 1/\sigma = 2.9 \pm 0.3 \qquad (d = 2). \tag{A6b}$$

In $1 + 1$ dimensions the value of σ is in good agreement with the predictions of DP, $1/\sigma \simeq 2.83$. However, the values of γ_p and β_p differ from the predictions of DP. This is not surprising since the definitions of clusters in both models are quite different. For the DPD model the clusters are the avalanches (compact regions confined between two DP paths), while the DP cluster are branchy trees comprised of directed paths.

In percolation theory, the correlation lengths are defined through the formulas

$$\xi_{\perp}^2 \equiv \frac{\langle s R_{\perp}^2 \rangle}{\langle s \rangle} \sim (p_c - p)^{-2\nu_{\perp}}, \tag{A7a}$$

$$\xi_{\parallel}^2 \equiv \frac{\langle s R_{\parallel}^2 \rangle}{\langle s \rangle} \sim (p_c - p)^{-2\nu_{\parallel}}, \tag{A7b}$$

where the angular brackets denote an average of realizations of the disorder and $R_{\perp}^2$ and $R_{\parallel}^2$ are the perpendicular and the parallel components of the square of the radius of gyration of the avalanches

$$R_{\perp}^2 \equiv \overline{h^2} - \overline{h}^2, \tag{A8a}$$

$$R_{\parallel}^2 \equiv \overline{x^2} - \overline{x}^2, \tag{A8b}$$

where the overbar denotes a spatial average for all cells of the avalanche in a given realization of the disorder. The relations (A7b) and (A8b) were applied to the calculation of the correlation length exponents presented in Sec. IV. The results obtained are in good agreement with theoretical calculations for DP in $1 + 1$ dimensions.

APPENDIX B: CALCULATING THE VELOCITY EXPONENT

The purpose of this appendix is to propose an alternative method for the calculation of the velocity exponent θ. The traditional way to calculate θ is to monitor the average height of the interface after the system becomes saturated. This is a very time consuming procedure for two reasons. First, the dependence of the saturation time $t_{\times}$ on the system size $t_{\times} \sim L^z$ leads to an great increase in computation time when we use large system sizes. Second, the large fluctuations in the velocity of about its average value leads to an increase in the number of runs required for achieving good statistics. The reason for the large fluctuations of the velocity are due to the fact that, near the transition, the motion of the interface is not smooth but rather is very "jerky," i.e., short periods of jumpy motion are followed by long periods of near immobility.

We assume that, before saturation, the velocity scales with time as a power law with an exponent ψ

$$v(t, f) \sim t^{-\psi} f_5(t/t_{\times}), \tag{B1}$$

with $t_{\times} \sim \xi_{\parallel}^z$. A comparison of (B1) with (1.6) implies that $f_5(u)$ is a scaling function that satisfies $f_5(u \ll 1) = \text{const}$, and $f_5(u \gg 1) \sim u^{\psi}$ and that

$$\theta = \nu_{\parallel} \, z \, \psi. \tag{B2}$$

The calculation of the exponents ψ, z, and $\nu_{\parallel}$ then allows us to estimate θ. Numerical tests reveal that (B2) is well obeyed.

Relation (B2) can be combined with (3.9), leading to the scaling law

$$\psi = 1 - \beta. \tag{B3}$$

This relation provides an alternate method to check the consistency of the scaling laws derived in the text.

[1] T. Vicsek, *Fractal Growth Phenomena*, 2nd ed. (World Scientific, Singapore, 1992), Pt. IV; *Dynamics of Fractal Surfaces*, edited by F. Family and T. Vicsek (World Scientific, Singapore, 1991); J. Kertész and T. Vicsek, in *Fractals in Science*, edited by A. Bunde and S. Havlin (Springer-Verlag, Heidelberg, 1994).

[2] J. Krug and H. Spohn, in *Solids Far From Equilibrium: Growth, Morphology and Defects*, edited by C. Godréche

(Cambridge University Press, Cambridge, 1991).
[3] P. Meakin, Phys. Rep. **235**, 189 (1993).
[4] T. Halpin-Healey and Y.-C. Zhang, Phys. Rep. **254**, 215 (1995).
[5] A.-L. Barabási and H. E. Stanley, *Fractal Concepts in Surface Growth* (Cambridge University Press, Cambridge, 1995).
[6] J.-F. Gouyet, M. Rosso and B. Sapoval, in *Fractals and Disordered Systems*, edited by A. Bunde and S. Havlin (Springer-Verlag, Heidelberg, 1991).
[7] J. P. Stokes, A. P. Kushnick, and M. O. Robbins, Phys. Rev. Lett. **60**, 1386 (1988).
[8] M. A. Rubio, C. A. Edwards, A. Dougherty, and J. P. Gollub, Phys. Rev. Lett. **63**, 1685 (1989); V. K. Horváth, F. Family, and T. Vicsek, *ibid.* **65**, 1388 (1990); M. A. Rubio, C. A. Edwards, A. Dougherty, and J. P. Gollub, *ibid.* **65**, 1389 (1990).
[9] T. Vicsek, M. Cserzö, and V. K. Horváth, Physica A **167**, 315 (1990).
[10] V. K. Horváth, F. Family, and T. Vicsek, J. Phys. A **24**, L25 (1991); Phys. Rev. Lett. **67**, 3207 (1991).
[11] S. He, G. L. M. K. S. Kahanda, and P.-z. Wong, Phys. Rev. Lett. **69**, 3731 (1992).
[12] J. Zhang, Y.-C. Zhang, P. Alstrøm, and M. T. Levinsen, Physica A **189**, 383 (1992).
[13] S. Havlin, A.-L. Barabási, S. V. Buldyrev, C. K. Peng, M. Schwartz, H. E. Stanley, and T. Vicsek, in *Growth Patterns in Physical Sciences and Biology*, Proceedings of the NATO Advanced Research Workshop, Granada, 1991, edited by J. M. Garcia-Ruiz, E. Louis, P. Meakin, and L. M. Sander (Plenum, New York, 1993).
[14] S. V. Buldyrev, A.-L. Barabási, S. Havlin, F. Caserta, H. E. Stanley, and T. Vicsek, Phys. Rev. A **45**, R8313 (1992).
[15] S. V. Buldyrev, A.-L. Barabási, S. Havlin, J. Kertész, H. E. Stanley, and H. S. Xenias, Physica A **191**, 220 (1992); A.-L. Barabási, S. V. Buldyrev, S. Havlin, G. Huber, H. E. Stanley, and T. Vicsek, in *Surface Disordering: Growth, Roughening and Phase Transitions*, edited by R. Jullien, J. Kertész, P. Meakin, and D. E. Wolf (Nova Science, Commack, 1992).
[16] S. V. Buldyrev, S. Havlin, and H. E. Stanley, Physica A **200**, 200 (1993); S. V. Buldyrev, S. Havlin, J. Kertész, A. Shehter, and H. E. Stanley, Fractals **1**, 827 (1993).
[17] L. A. N. Amaral, A.-L. Barabási, S. V. Buldyrev, S. Havlin, and H. E. Stanley, Phys. Rev. Lett. **72**, 641 (1994); Fractals **1**, 818 (1993).
[18] F. Family and T. Vicsek, J. Phys. A **18**, L75 (1985).
[19] F. Family, J. Phys. A **19**, L441 (1986).
[20] P. Meakin, P. Ramanlal, L. M. Sander, and R. C. Ball, Phys. Rev. A **34**, 5091 (1986).
[21] J. M. Kim and J. M. Kosterlitz, Phys. Rev. Lett. **62**, 2289 (1989).
[22] S. F. Edwards and D. R. Wilkinson, Proc. R. Soc. London Ser. A **381**, 17 (1982).
[23] M. Kardar, G. Parisi, and Y.-C. Zhang, Phys. Rev. Lett. **56**, 889 (1986).
[24] E. Medina, T. Hwa, M. Kardar, and Y.-C. Zhang, Phys. Rev. A **39**, 3053 (1989); C. K. Peng, S. Havlin, M. Schwartz, and H. E. Stanley, *ibid.* **44**, 2239 (1991); J. G. Amar, P.-M. Lam, and F. Family, *ibid.* **43**, 4548 (1991).
[25] Y.-C. Zhang, J. Phys. (Paris) **51**, 2129 (1990); S. V. Buldyrev, S. Havlin, J. Kertész, H. E. Stanley, and T. Vicsek, Phys. Rev. A **43**, 7113 (1991); S. Havlin, S. V. Buldyrev, H. E. Stanley, and G. H. Weiss, J. Phys. A **24**, L925 (1991).
[26] A.-L. Barabási, Phys. Rev. A **46**, R2977 (1992).
[27] L.-H. Tang and H. Leschhorn, Phys. Rev. A **45**, R8309 (1992).
[28] M. Cieplak and M. O. Robbins, Phys. Rev. Lett. **60**, 2042 (1988); N. Martys, M. Cieplak, and M. O. Robbins, *ibid.* **66**, 1058 (1991).
[29] C. S. Nolle, B. Koiller, N. Martys, and M. O. Robbins, Phys. Rev. Lett. **71**, 2074 (1993); B. Koiller, M. O. Robbins, H. Ji, and C. S. Nolle, in *New Trends in Magnetic Materials and their Applications*, edited by J. L. Moran-Lopez and J. M. Sanchez (Plenum, New York, 1993).
[30] D. A. Kessler, H. Levine, and Y. Tu, Phys. Rev. A **43**, 4551 (1991).
[31] G. Parisi, Europhys. Lett. **17**, 673 (1992); L. A. N. Amaral (unpublished).
[32] H. Leschhorn, Physica A **195**, 324 (1993).
[33] M. Dong, M. C. Marchetti, A. A. Middleton, and V. Vinokur, Phys. Rev. Lett. **70**, 662 (1993).
[34] M. Benoit and R. Jullien, Physica A **207**, 500 (1994).
[35] D. Spasojevic and P. Alstrøm, Physica A **201**, 482 (1993).
[36] Z. Csahók, K. Honda, and T. Vicsek, J. Phys. A **26**, L171 (1993); Z. Csahók, K. Honda, E. Somfai, M. Vicsek, and T. Vicsek, Physica A **200**, 136 (1993).
[37] L. A. N. Amaral, A.-L. Barabási, and H. E. Stanley, Phys. Rev. Lett. **73**, 62 (1994); H. A. Makse, A.-L. Barabási, and H. E. Stanley (unpublished).
[38] L.-H. Tang, M. Kardar, and D. Dhar, Phys. Rev. Lett. **74**, 920 (1995).
[39] H. A. Makse and L. A. N. Amaral (unpublished).
[40] T. Nattermann, S. Stepanov, L.-H. Tang, and H. Leschhorn, J. Phys. (France) II **2**, 1483 (1992).
[41] O. Narayan and D. S. Fisher, Phys. Rev. B **48**, 7030 (1993).
[42] R. Bruinsma and G. Aeppli, Phys. Rev. Lett. **52**, 1547 (1984).
[43] K. Sneppen, Phys. Rev. Lett. **69**, 3539 (1992); L.-H. Tang and H. Leschhorn, *ibid.* **70**, 3832 (1993); K. Sneppen and M. H. Jensen, *ibid.* **70**, 3833 (1993).
[44] K. Sneppen and M. H. Jensen, Phys. Rev. Lett. **71**, 101 (1993).
[45] H. Leschhorn and L.-H. Tang, Phys. Rev. E **49**, 1238 (1994).
[46] Z. Olami, I. Procaccia, and R. Zeitak, Phys. Rev. E **49**, 1232 (1994).
[47] S. Maslov and M. Paczuski, Phys. Rev. E **50**, R643 (1994).
[48] P. Bak, C. Tang, and K. Wiesenfeld, Phys. Rev. Lett. **59**, 381 (1987).
[49] P. Bak and K. Sneppen, Phys. Rev. Lett. **71**, 4083 (1993); M. Paczuski, S. Maslov, and P. Bak, Europhys. Lett. **27**, 96 (1994); S. Maslov, M. Paczuski, and P. Bak, Phys. Rev. Lett. **73**, 2162 (1994).
[50] T. Ray and N. Jan, Phys. Rev. Lett. **72**, 4045 (1994); B. Jovanović, S. V. Buldyrev, S. Havlin, and H. E. Stanley, Phys. Rev. E **50**, R2403 (1994).
[51] B. Suki, A.-L. Barabási, Z. Hantos, F. Peták, and H. E. Stanley, Nature **368**, 615 (1994).
[52] Smaller pinning regions might become totally surrounded by the wet region. However, because of the surface tension that acts to decrease the size of the interface between the wet and the dry regions, these dry "islands" inside

the wet region eventually become wet.

[53] We introduce this time-dependent randomness in the model to mimic the experimental fact that for $F > F_c$ a transition to the KPZ behavior with annealed disorder is observed for $\ell \gg \xi$. For smaller length scales the effect of this annealed randomness is irrelevant.

[54] The justification of this particular rule lies not only on the computational simplifications that it affords but also on the experimental finding that overhangs do not play an important role in the scaling properties of the interface for imbibition.

[55] D. Stauffer and A. Aharony, *Introduction to Percolation Theory*, 2nd ed. (Taylor & Francis, London, 1992).

[56] *Fractals and Disordered Systems* (Ref. [6]); S. Havlin and D. Ben-Avraham, Adv. Phys. **36**, 695 (1987).

[57] J. W. Essam, K. De'Bell, J. Adler, and F. M. Bhatti, Phys. Rev. B **33**, 1982 (1986); J. W. Essam, A. J. Guttmann, and K. De'Bell, J. Phys. A **21**, 3815 (1988).

[58] S. Havlin, L. A. N. Amaral, S. V. Buldyrev, S. T. Harrington, and H. E. Stanley, Phys. Rev. Lett. (to be published).

[59] We found that the values of z could be well approximated by the mnemonic formula $z = 2-[(6-d)/5]^{3/4}$. Although this expression is incompatible with an ϵ expansion and so cannot be correct, it can be useful in the estimation of the exponents.

[60] For the study of the avalanches it is more convenient to consider a new definition of the unit time in which, for each time step, all unblocked nearest neighbors to the invading region also become invaded. This means that we make a parallel updating of the system. For p close to p_c, this produces no changes in the results; however, for $p \ll p_c$ this parallel updating leads to an essentially flat interface.

[61] S. V. Buldyrev, S. Havlin, J. Kertész, R. Sadr, A. Shehter, and H. E. Stanley (unpublished); see also the application of the Cayley tree to avalanches in lung inflation [B. Suki, A.-L. Barabasi, S. V. Buldyrev, and H. E. Stanley (unpublished)].

[62] This definition of time results in multiaffine [63] scaling of the time-dependent height-height correlation functions [44].

[63] A.-L. Barabási and T. Vicsek, Phys. Rev. A **44**, 2730 (1991); A.-L. Barabási, P. Szépfalusy, and T. Vicsek, Physica A **178**, 17 (1991).

[64] In this work we refer to evaporation as the origin of the gradient. However, other factors also affect the value of the experimental gradient, among them the density of the suspension. Indeed, our experiments confirm this idea and suggest that the model accounts for all these effects.

[65] We stress the fact that the actual disorder in the paper is height independent. However, due to the decrease in capillary pressure with height, the *effect* of the inhomogeneities is increasing with height. In the model we take account of this changing balance between capillary pressure and strength of the inhomogeneities by introducing a gradient in the "effective" density of pinning obstacles.

[66] B. Sapoval, M. Rosso, and J. F. Gouyet, J. Phys. (Paris) Lett. **46**, L149 (1985); M. Rosso, J. F. Gouyet, and B. Sapoval, Phys. Rev. Lett. **57**, 3195 (1986).

[67] D. Wilkinson, Phys. Rev. A **30**, 520 (1984); **34**, 1380 (1986).

[68] A. Birovljev, L. Furuberg, J. Feder, T. Jøssang, K. J. Måløy, and A. Aharony, Phys. Rev. Lett. **67**, 584 (1991).

[69] A. Hansen, T. Aukrust, J. M. Houlrik, and I. Webman, J. Phys. A **23**, L145 (1990); A. Hansen and J. M. Houlrik, *ibid.* **24**, 2377 (1991).

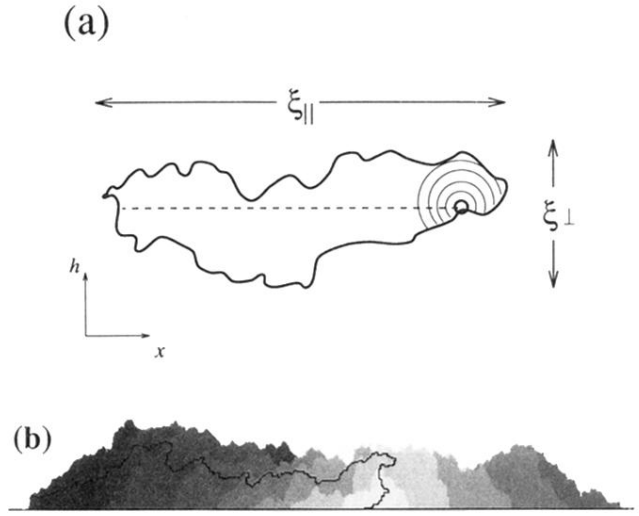

FIG. 10. Illustration of the dynamics of the DPD model for $1+1$ dimensions. (a) *Schematic representation* of a region defined by two pinning paths. The heavy circle indicates the origin for the invasion, the thin arcs represent the positions of the invading front at successive times, and the dashed line represents schematically the path for the invasion. (b) *Simulation* results for invasion after 2^{10} time steps starting from a single cell near the center. We show the invaded region at a sequence of times that are multiples of 128. Regions invaded at later times are displayed in darker shades of gray. The path from the origin to the latest invaded point is shown in black. Although this path displays some fluctuations in the vertical direction, they can be disregarded since $\nu_{\|} > \nu_{\perp}$, so as $p \to p_c$, $\xi_{\perp}/\xi_{\|} \to 0$. Thus the distance propagated by the invading front is proportional to time. Since $t_{\times} \sim \ell$, we can conclude that $z = d_{\min} = 1$.

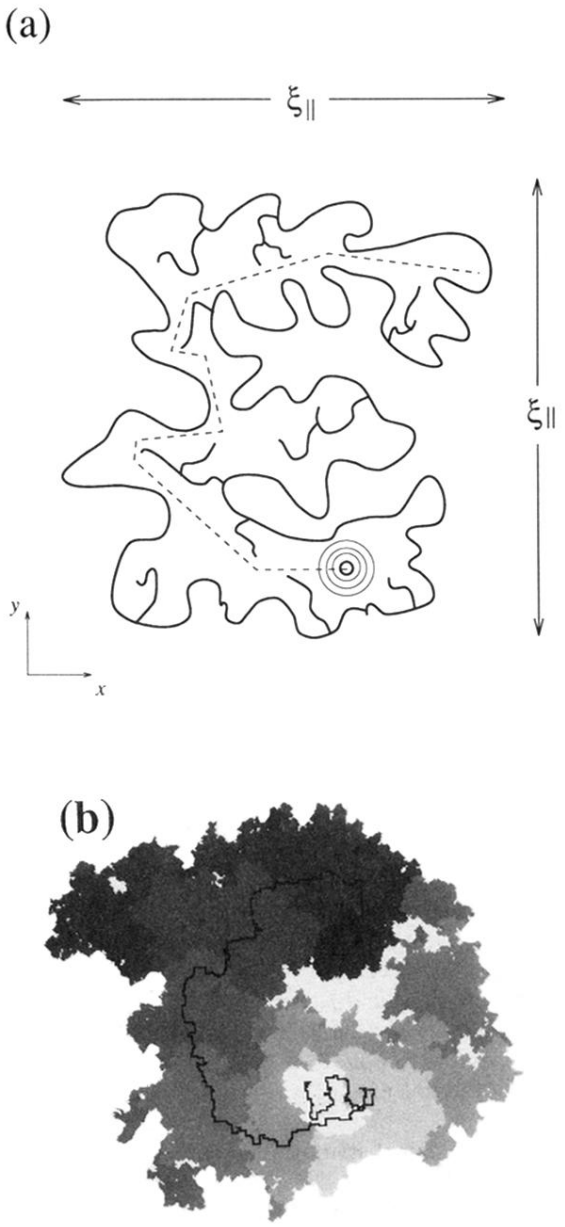

FIG. 11. Illustration of the dynamics of the DPD model for $2+1$ dimensions. (a) *Schematic representation* of the xy projection of the region defined by two pinning self-affine DSs. The heavy circle indicates the origin for the invasion, the thin arcs represent the xy projections of the invading front at successive times, and the dashed line represents schematically the path for the invasion. (b) *Simulation* results for invasion after 2^{10} time steps starting from a single cell located to the left of the center. We show the xy projection of the invaded region at a sequence of times that are multiples of 128. Regions invaded at later times are displayed in darker shades of gray. It is visually apparent that it takes a long time to invade some regions close to the origin because the path to that position (shown in black) appears to be a fractal curve of dimension greater than one. The fluctuations in the vertical direction can be disregarded since we know that $\xi_{\perp}/\xi_{\parallel} \to 0$. We find that the path can be identified with the shortest path (the "chemical distance") of isotropic percolation and that its length scales with the linear distance r to the point as $r^{d_{\min}}$.

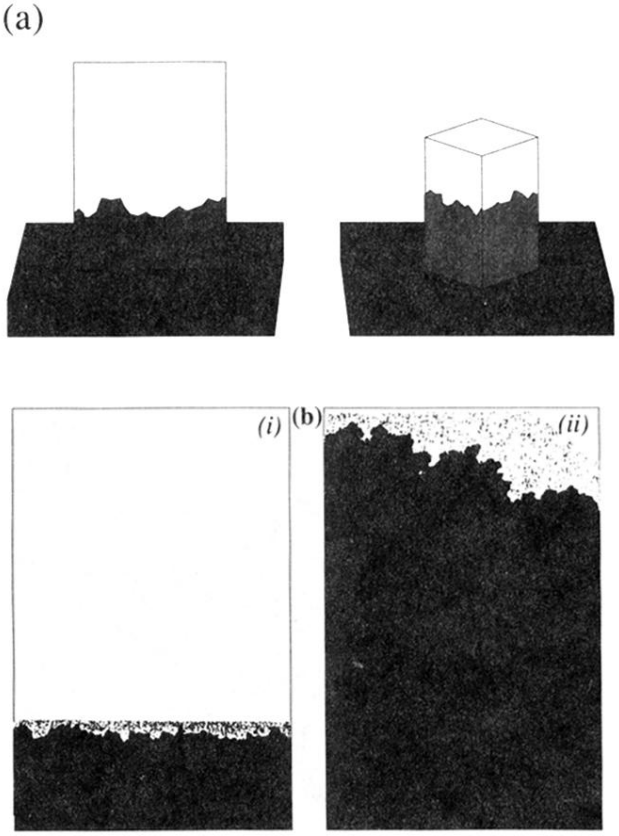

FIG. 2. (a) Schematic illustration of the experimental setup. In the 1+1-dimensional experiments we use paper towels as the disordered media and coffee as the invading fluid. The edge of the paper towels is 20 cm. (b) Photographs of pinned interfaces in imbibition experiments with coffee and paper towels for (i) a high evaporation rate $g_{\rm expt} = 0.94 g_0$ and (ii) a low evaporation rate $g_{\rm expt} = 0.25 g_0$. Here g_0 is the undetermined multiplicative constant discussed in Sec. V.

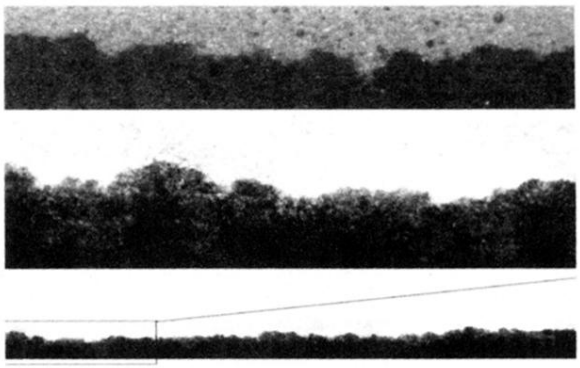

FIG. 4. Digitized ink interface in the (a) Oasis brick and (b) paper roll using an Apple computer scanner with a resolution of 300 pixels per inch. In (c) we show the full image from which (b) was magnified. The brick has a section of 7×7 cm^2 and the paper roll an exterior radius of 7.5 cm and an interior radius of 1.75 cm.

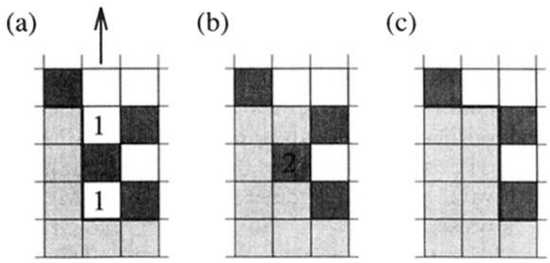

FIG. 6. Example of the application of the growth rule to a particular configuration of the interface. White squares refer to dry unblocked cells, the darker squares refer to dry blocked cells, and the gray squares refer to wet cells. The tick line shows the position of the interface. Let us suppose that the column indicated by the arrow in (a) was chosen for growth. According to our model, the cells marked 1 will become wet because they are nearest neighbors to the wet region. After the wetting, we can see in (b) that the cell marked 2 is below a wet cell, applying the rule to erode any overhang we wet that cell. In (c) we show the configuration of the interface after the growth (thick line).

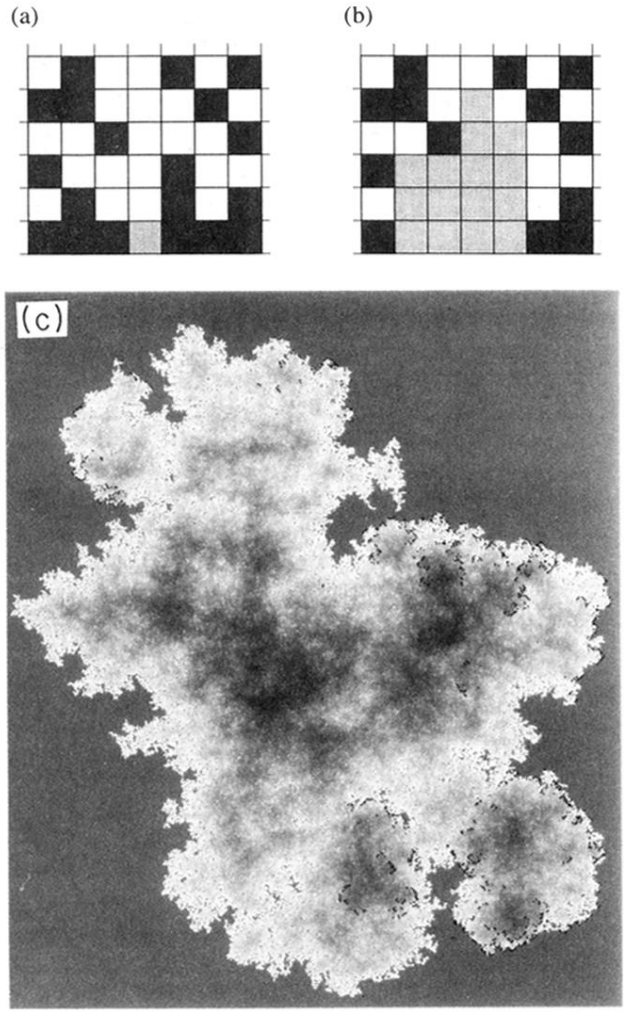

FIG. 9. (a) Initial conditions in the DPD model for the growth of single avalanches: all sites in the bottom edge except one are blocked. The color convention for the cells is the same as in Fig. 6. (b) The wet region after some time; the quantity $n(t)$ defined in the text counts the number of unblocked cells in the interface, in this case 8. (c) Horizontal projection of an avalanche in $2+1$ dimensions for $p \simeq p_c$. The avalanche was started at the center of the figure and is shown at time 2^{10}. The current diameter of the cluster is approximately 2^{10}. The uniform gray area shows the region left dry since the beginning of the process. The darkest shade of gray corresponds to the largest heights of the interface. The black dots, forming a "fractal dust," indicate the unblocked cells at the interface.